

AD-A163 005

TURBULENT FLOW OVER ROUGH TURBINE AIRFOILS(U) OHIO  
STATE UNIV RESEARCH FOUNDATION COLUMBUS L 5 JAN AUG 85  
OSURF-763057/714467 AFMRL-TR-85-2056 F33615-82-K-2218

1/1

UNCLASSIFIED

F/G 20/4

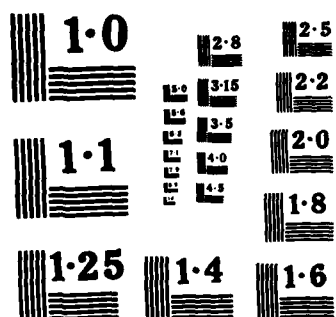
NL

END

FORMED

BY

DATE



NATIONAL BUREAU OF STANDARDS  
MICROCOPY RESOLUTION TEST CHART

2

AFWAL-TR-85-2056

\*TURBULENT FLOW OVER ROUGH TURBINE AIRFOILS



Lit S. Han

Department of Mechanical Engineering  
The Ohio State University  
1314 Kinnear Road  
Columbus, Ohio 43212

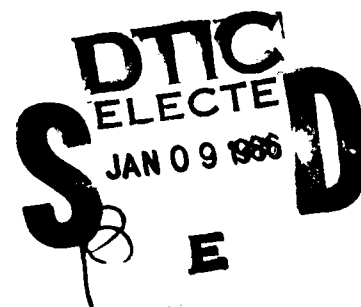
August 1985

Final Report for Period June 1983 - December 1984

APPROVED FOR PUBLIC RELEASE; DISTRIBUTION UNLIMITED.

AERC PROPULSION LABORATORY  
AIR FORCE WRIGHT AERONAUTICAL LABORATORIES  
AIR FORCE SYSTEMS COMMAND  
WRIGHT PATTERSON AIR FORCE BASE, OHIO 45433

(\*Funded in Part by NASA Lewis Research Center)



AD-A163 005

DTIC FILE COPY

86 1 9 080

NOTICE

When Government drawings, specifications, or other data are used for any purpose other than in connection with a definitely related Government procurement operation, the United States Government thereby incurs no responsibility nor any obligation whatsoever; and the fact that the government may have formulated, furnished, or in any way supplied the said drawings, specifications, or other data, is not to be regarded by implication or otherwise as in any manner licensing the holder or any other person or corporation, or conveying any rights or permission to manufacture use, or sell any patented invention that may in any way be related thereto.

This report has been reviewed by the Office of Public Affairs (ASD/PA) and is releasable to the National Technical Information Service (NTIS). At NTIS, it will be available to the general public, including foreign nations.

This technical report has been reviewed and is approved for publication.

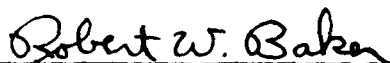


CHARLES D. MACARTHUR  
Project Engineer



MICHAEL E. STEFKOVICH, Major, USAF  
Chief, Components Branch

FOR THE COMMANDER



ROBERT W. BAKER, Major, USAF  
Deputy Director  
Turbine Engine Division  
Aero Propulsion Laboratory

"If your address has changed, if you wish to be removed from our mailing list, or if the addressee is no longer employed by your organization please notify AFWAL/POTC, W-PAFB, OH 45433 to help us maintain a current mailing list".

Copies of this report should not be returned unless return is required by security considerations, contractual obligations, or notice on a specific document.

Unclassified

SECURITY CLASSIFICATION OF THIS PAGE

AD-A163 005

## REPORT DOCUMENTATION PAGE

1a. REPORT SECURITY CLASSIFICATION Unclassified		1b. RESTRICTIVE MARKINGS									
2a. SECURITY CLASSIFICATION AUTHORITY		3. DISTRIBUTION/AVAILABILITY OF REPORT Approved for public release; distribution unlimited									
2b. DECLASSIFICATION/DOWNGRADING SCHEDULE											
4. PERFORMING ORGANIZATION REPORT NUMBER(S) 763057/714467		5. MONITORING ORGANIZATION REPORT NUMBER(S) AFWAL-TR-85-2056									
6a. NAME OF PERFORMING ORGANIZATION The Ohio State University Research Foundation	6b. OFFICE SYMBOL (If applicable) AFWAL/POTC	7a. NAME OF MONITORING ORGANIZATION Air Force Wright Aeronautical Laboratories, Aero Propulsion Laboratory (AFWAL/POTC)									
6c. ADDRESS (City, State and ZIP Code) 1314 Kinnear Road Columbus, Ohio 43212		7b. ADDRESS (City, State and ZIP Code) Wright Patterson Air Force Base, OH 45433									
8a. NAME OF FUNDING/SPONSORING ORGANIZATION Aero Propulsion Laboratory	8b. OFFICE SYMBOL (If applicable) AFWAL/POTC	9. PROCUREMENT INSTRUMENT IDENTIFICATION NUMBER In part under MIPR-C-79073-D F33615-82-K-2218									
8c. ADDRESS (City, State and ZIP Code) Wright Patterson Air Force Base, OH 45433		10. SOURCE OF FUNDING NOS. <table border="1"><thead><tr><th>PROGRAM ELEMENT NO.</th><th>PROJECT NO.</th><th>TASK NO.</th><th>WORK UNIT NO.</th></tr></thead><tbody><tr><td>62203F</td><td>3066</td><td>14</td><td>11</td></tr></tbody></table>		PROGRAM ELEMENT NO.	PROJECT NO.	TASK NO.	WORK UNIT NO.	62203F	3066	14	11
PROGRAM ELEMENT NO.	PROJECT NO.	TASK NO.	WORK UNIT NO.								
62203F	3066	14	11								
11. TITLE (Include Security Classification) Turbulent Flow Over Rough Turbine Airfoils											
12. PERSONAL AUTHOR(S) Dr. Lit S. Han, Professor of Mechanical Engineering, The Ohio State University											
13a. TYPE OF REPORT Final	13b. TIME COVERED FROM 6/83 TO 12/84	14. DATE OF REPORT (Yr., Mo., Day) August 1985	15. PAGE COUNT 85								
16. SUPPLEMENTARY NOTATION * Funded in Part by NASA Lewis Research Center, Cleveland OH 44135											
17. COSATI CODES <table border="1"><thead><tr><th>FIELD</th><th>GROUP</th><th>SUB. GR.</th></tr></thead><tbody><tr><td>21</td><td>05</td><td></td></tr></tbody></table>		FIELD	GROUP	SUB. GR.	21	05		18. SUBJECT TERMS (Continue on reverse if necessary and identify by block number) Turbine blades; vanes; surface roughness; turbulent boundary layer; skin friction. ←			
FIELD	GROUP	SUB. GR.									
21	05										
19. ABSTRACT (Continue on reverse if necessary and identify by block number) → A methodology to analyze turbulent boundary layer over rough turbine vanes or blades is developed. A new formulation of the mixing length model, expressed in the velocity-space variable, is instrumental in the modeling effort, and the surface roughness effect is embedded in an amplification factor as a multiplier to the mixing length. (The amplification factor ranges from unity for a smooth surface upward for rough surfaces, with its variation depending on the type of the roughness). For demonstration, the new methodology is applied to the analysis of turbulent flow over a flat plate with two surface roughnesses. For a plate length with a length Reynolds number of $10^7$ , skin friction is increased by as much as 60 percent, if the roughness-to-length ratio is $10^{-4}$ . Keywords: <i>Reynolds number, skin friction, roughness, turbulent flow</i>											
20. DISTRIBUTION/AVAILABILITY OF ABSTRACT UNCLASSIFIED/UNLIMITED <input checked="" type="checkbox"/> SAME AS RPT. <input type="checkbox"/> DTIC USERS <input type="checkbox"/>		21. ABSTRACT SECURITY CLASSIFICATION Unclassified									
22a. NAME OF RESPONSIBLE INDIVIDUAL Charles D. MacArthur		22b. TELEPHONE NUMBER (Include Area Code) (513) 255-4830	22c. OFFICE SYMBOL AFWAL/POTC								

## FOREWORD

The environment envisioned for gas turbine engines of the near future includes gas streams at higher temperatures, carrying particulate matters and using different fuels. These factors would cause roughness patterns on the airfoil surfaces and consequently would degrade the engine performance, as a number of tests have already confirmed. Thus a capability is needed to analyze and hence to predict the surface roughness effects.

This investigation is a first step to answer this need. It is a part of an overall program which has the objective of establishing a fundamental methodology to address the problem of increased friction and heat transfer over surfaces with roughnesses. This report covers the first phase of the overall program and is concerned with the analysis and calculation of the turbulent boundary layers. A second phase will focus on the heat transfer aspect and other factors not treated in this report.

Support for the continuing investigation was provided by the Turbine Engine Division, Aero Propulsion Laboratory, U.S. Air Force. The project was monitored by Dr. Kervyn Mach and Mr. Charles MacArthur, AFWAL/POTC. Their assistance is appreciated by the author of this report.

Accession For	
NTIS GRA&I	<input checked="" type="checkbox"/>
DTIC TAB	<input type="checkbox"/>
Unannounced	<input type="checkbox"/>
Justification	
By _____	
Distribution/	
Availability Codes	
Dist	Avail and/or Special
A-1	



## TABLE OF CONTENTS

	<u>Page</u>
I. INTRODUCTION	1
II. THE MIXING LENGTH AND SURFACE ROUGHNESS	7
2.1 Prandtl's Formulation Reviewed	7
2.2 Recent Modifications for Rough Surfaces	11
2.3 A New Formulation for Smooth Surfaces	13
2.4 Extension to Rough Surfaces	20
2.5 Preferred Model Formulations	22
III. THE ROUGHNESS AMPLIFICATION FACTOR	27
3.1 Amplification Factors for Nikuradse' Sandgrain Roughnesses	29
3.2 Other Types of Roughnesses: Moody, Colebrook- White, Hama	36
3.3 Spatial Distributions of Velocity and Mixing Length Ratio	40
IV. FLOW OVER A ROUGH FLAT PLATE	51
V. CONCLUSIONS	63
REFERENCES	67
APPENDIX   Computer Program for Turbulent Boundary Layer Analysis	71

# LIST OF ILLUSTRATIONS

	<u>Page</u>
Figure 1 Comparative Velocity Profiles with Wall-Law $u^+ = 5.75 \log_{10} y^+ + 5.24$ ( $K = 0.4$ , $E = 8.134$ )	18
Figure 2 Comparison of Smooth-Surface Data with Various Formulations	19
Figure 3 Comparison of Robertson's Data with Calculated Profiles, Model for Turbulent Viscosity (i)	24
Figure 4 Comparison of Robertson's Data with Calculated Profiles, Model for Turbulent Viscosity (iii)	25
Figure 5 Comparison of Robertson's Data with Calculated Profiles, Model for Mixing Length (iv)	26
Figure 6 Distribution of Velocity-Shift Function B vs Roughness Reynolds Number $k_s^+$	43
Figure 7 Calculated Pipe Friction Factors for Nikuradse' Sandgrain Roughnesses	44
Figure 8a Mixing Length Amplification vs. Surface Roughness, Low Range	45
Figure 8b Mixing Length Amplification vs. Surface Roughness	46



# LIST OF ILLUSTRATIONS (concluded)

	<u>Page</u>
Figure 9    Calculated Pipe Friction Factors for Commercial-Random Roughnesses, (Moody)	47
Figure 10   Wall-Region Velocities for Rough Surfaces (Colebrook-White)	48
Figure 11   Spatial Distribution of Rough-to-Smooth Mixing Length Ratio	49
Figure 12   Calculated Local Friction Coefficients on Flat Plates with Nikuradse' Sandgrain Roughnesses ( $K=0.41$ , $E=7.768$ )	54
Figure 13   Calculated Momentum Thicknesses vs. Reynolds Numbers with Nikuradse' Sandgrain Roughnesses ( $K=0.41$ , $E=7.768$ )	55
Figure 14   Calculated Rough-Surface Boundary Layer Velocity Profiles at $Re_x = 10^7$ , Boundary-Layer Coordinates ( $K=0.41$ , $E=7.768$ )	56
Figure 15   Calculated Rough-Surface Boundary Layer Velocity Profiles at $Re_x = 10^7$ , Plus-Coordinate ( $K=0.41$ , $E=7.768$ )	57
Figure A-1   Grid Network for 3-Point 2-Station Marching	75

# LIST OF SYMBOLS AND ABBREVIATIONS

## NOMENCLATURE

- A = van Driest's damping factor ( $= 26$ ), equation (5)
- B = Nikuradse intercept-function, equation (27)
- C = wall-law intercept for smooth walls, equation (1)
- $C_f$  = local surface friction coefficient ( $\tau / \frac{1}{2} \rho U_e^2$ )
- D = van Driest damping factor, equation (5)
- E = wall-law constant, exponential form, equation (1a)
- f = Darcy's friction factor,  $8(u_t/u_a)^2$
- $k_s$  = wall roughness height
- $k_s^+$  = roughness Reynolds number ( $k_s u_t / \nu$ )
- K = wall-law (von Karman) constant ( $0.40 \sim 0.411$ )
- $l$  = mixing length
- $l^+$  = dimensionless mixing length ( $l u_t / \nu$ )
- $r_o$  = pipe radius
- $r_o^+$  = non-dimensional pipe radius, ( $r_o u_t / \nu$ )
- R = amplification factor
- $Re$  = pipe flow Reynolds number, ( $2u_a r_o / \nu$ )
- $Re_x$  = distance Reynolds number ( $x U_e / \nu$ )
- u = time-averaged turbulent velocity parallel to a wall
- $u_a$  = cross-section averaged velocity of u
- $u_t$  = friction velocity ( $\sqrt{\tau / \rho}$ )
- $u^+$  = dimensionless velocity ( $u / u_t$ )
- $U_e$  = freestream velocity
- x = distance along a flat plate
- $\bar{x}$  = ( $x U_e / \nu$ )
- y = distance from wall

#### LIST OF SYMBOLS AND ABBREVIATIONS (concluded)

- $y^+$  = dimensionless normal distance ( $y u_e / \nu$ )  
 $\bar{y}$  = ( $y U_e / \nu$ )

#### Greek Symbols

- $\delta$  = marching-direction grid space, see Figure A.1  
 $\delta_1$  = displacement thickness  
 $\bar{\delta}_1$  = ( $\delta_1 u_e / \nu$ )  
 $\Delta$  = transverse grid space, see Figure A.1  
 $\Delta u^+$  = magnitude of asymptotic downshift of  $u^+$   
 $\epsilon^+$  = turbulent viscosity/molecular viscosity ( $\mu_t / \mu$ )  
 $\gamma$  = transverse grid spacing ratio (1.07)  
 $\rho$  = fluid density  
 $\tau$  = wall shear stress  
 $\nu$  = kinematic viscosity of fluid  
 $\mu_t$  = turbulent viscosity  
 $\mu$  = molecular viscosity

#### Subscripts

- a = average  
e = established; boundary layer edge  
t = frictional; turbulent  
w = wall

## I. INTRODUCTION

The condition of a solid surface which may be as-manufactured or as a result of its service exposure may exhibit asperities varying in magnitude and texture from one surface to another. For practical purposes, all surfaces may be considered rough. A rough surface exerts two fluid dynamic effects on the flow adjacent to it: it promotes and oftentimes triggers flow transition from a laminar boundary layer to a turbulent one; and it increases flow resistance, particularly in turbulent flow which prevails much more frequently than laminar flow.

Of these two effects, the first one, though having been long recognized, has not been extensively investigated until in recent years. Roughness-induced transition began to attract notice in connection with problems such as those encountered by re-entry vehicles when their nose-tips were cooled by ablation, resulting in an irregular surface appearance. The rough texture of the surfaces causes turbulent boundary layers to form very near, or at, the nose stagnation point. The turbulent flow thus transformed may alter the aerodynamics of the vehicle as a whole; also, the increased heating rate is an undesirable by-product.

The second, but not secondary, effect caused by surface roughness has been known for a much longer time and has a much wider bearing on virtually all engineering disciplines wherever fluid flow is found. It is common knowledge that scrubbing a ship's hull to remove barnacles and weeds is translated into added speed for the seacraft; in hydraulic engineering, corrosion or erosion of pipes and conduits - despite their enlarged flow cross-sections - actually retards the flow; and in modern flight technology of recent decades, gas turbine engines operating with vitiated blades

are known to deteriorate in their performance. In these cited examples, the effect of surface roughness is adverse while in other instances in which heat transfer enhancement is the desired objective, surface roughness becomes favorable. In either event, and regardless of the purpose, a thorough understanding is indispensable to a quantitative analysis of the effect of roughness on the turbulent boundary layer adjacent to a surface and its attendant heat transfer. It is towards these two phenomena that this research program is directed.

The work reported here concerns itself with the analysis of turbulent boundary layers over rough surfaces. Extension to heat transfer will be taken up in the succeeding phase of the research program and will be reported later.

Historically, systematic, organized research on the role of surface irregularities on turbulent flow began in the Gottingen school of fluid mechanics. (An excellent description of the relevant work can be found in Bakhmeteff's book [1].) It was the pioneering work of Nikuradse on flow resistance in pipes coated with sandgrain roughnesses that had laid a foundation for the present state of knowledge. Apart from his numerical output - which is in itself significant - Nikuradse's work plus the interpretative insight of Prandtl revealed an important parameter, the roughness Reynolds number, as a vital link among the basic relationships governing the phenomenon. Since then, following the footsteps of Nikuradse and Prandtl, much has been added to the store of knowledge in the form of more test data, extensions and analyses. Noteworthy among these is the contribution by Moody [2], who analyzed and summarized well over 10,000 test data on flow through commercial pipes whose surfaces had various degrees of roughness. Using Darcy's definition of pipe friction factor, he

organized a convenient diagram, now known, most appropriately, as the Moody's friction factor chart, which can be found in almost all fluid mechanics textbooks.

Another significant extension, still in use today, is the work of Schlichting [3], who transposed Nikuradse' pipe-flow data to a flat-plate configuration, based on the supposition that the increase of surface friction due to roughness elements is independent of the external flow condition - a supposition whose validity for rough-surface flow has not been proven either by experiment or by analysis. Besides these cited investigations, there are other important contributions and they will be discussed in connection with the development of the present analysis as it proceeds.

The present work is motivated by gas turbine cooling technology which requires the consideration of the surface roughness characteristics of turbine blades or vanes (and compressor blade surfaces as well). The irregular surface asperities may result from thermal barrier coating or repeated impacts by particulate matter. Measurement of the momentum thickness on turbine airfoil surfaces by Bammert [4] demonstrated that surface roughnesses of the sizes that could reasonably be expected do play an appreciable role in affecting the overall parasitic drag and the performance loss. Additionally, a test program performed by AFLC concluded that a loss of 1 to 2 percent efficiency can be attributed to the surface roughness influence. From the gas turbine cooling viewpoint, increased heat transfer from the hot stream to the blade surfaces is even more of a critical concern than increased drag.

The need for further research is thus amply substantiated and is in fact pressing, giving the trend towards higher combustion temperatures and

reduced cooling air rates, at least as a goal to achieve. This research effort is to offer a unified view and an analytical approach for the analysis of turbulent boundary layers over rough surfaces. It does not, however, purport to unveil the microstructure of the turbulence caused by surface rough spots; rather it is concerned with the gross manifestations of the surface roughness elements in affecting the turbulent boundary layer flows.

The approach adopted is therefore semi-empirical, as is the case with most research efforts in turbulent shear flow. The present work starts with Prandtl's mixing length concept, but not his mathematical formulation. His simple but elucidating hypothesis, when incorporated into a differential equation for the time-averaged turbulent velocity, is now called the zero-equation model, as compared with more elaborate modeling efforts which are only beginning to emerge as a contending replacement. But in a large number of engineering problems, Prandtl's mixing length still retains its value because of its simplicity and expediency.

A distinguishing characteristic of this work is that the original mathematical formulation of Prandtl's mixing length expressed in the space coordinates is replaced by a new formulation in the velocity coordinates. In this new format, the effect of surface roughness is expressed via an amplification factor as a multiplier to the mixing length; the amplification factor ranges from 1 for a smooth surface upward as the surface roughness increases in size. Such an overall analytical structure is shown in the analysis to satisfy the conceptual requirement of more vigorous mixing in the near-surface region; and moreover, it is demonstrated by computation to comply with experimental evidence on the velocity distribution in the rough-wall turbulent boundary layers. The

concept of mixing length amplification modifying the new form of Prandtl's mixing length constitutes a basis of this work.



## II. THE MIXING LENGTH AND SURFACE ROUGHNESS

Nikuradse' rough-wall data plus those of other investigators over the subsequent years have firmly established that the law of the wall is as valid for turbulent boundary layers over rough surfaces as it is over smooth surfaces. A unique manifestation, however, is that in the wall-law region, an experimentally determined velocity distribution when non-dimensionalized by the plus-coordinate  $u^+ (=u/u_\tau)$  shows a definite, parallel downward shift from the wall-law for a smooth surface. The slope is unchanged. Thus, between the two boundary layers over the two types of surfaces, there is a difference and a similarity. Even though the region of the law of the wall is but a small fraction of the entire boundary layer thickness, it is the region in which maximum shear-turbulence and dissipation occurs. And in boundary layer flows, this region is relatively free from convective effects of the main flow (in terms of entrainment) and is characterized by a nearly constant stress condition.

In order to evolve a new mixing length formulation, it is necessary to recapitulate the essentials of Prandtl's original mixing length development so that certain matters can be cleared up.

### II.1 Prandtl's Formulation Reviewed

The widely accepted base for a semi-empirical, phenomenological description of shear flow over a solid, smooth wall is the logarithmic expression, now called the law of the wall,

$$u^+ = \frac{1}{K} \text{Log}_e y^+ + C \quad (1)$$

or,

$$u^+ = \frac{1}{K} \text{Log}_e E y^+, \quad (1a)$$

in which the constant coefficients K and C are approximately 0.4 and 5.5 respectively. The exponential constant E in Equation (1a) is but another representation of C, i.e.  $E = \exp(KC)$ .

Motivated, perhaps, by the universality of the correlation, Prandtl with his penetrating insight proposed a turbulent mixing length analogous to the mean free path in the kinetic theory of gases. In concept, it is the cross-stream distance traversed by a fluid lump before complete mixing and merging with the surrounding lumps. It then follows that turbulent shear stress resulting from such mixing can be expressed by a turbulent viscosity, again analogous to the molecular viscosity, by,

$$\tau = \mu_t (\partial u / \partial y). \quad (2)$$

Prandtl's hypothesis is finally in the form of

$$\mu_t = \rho l^2 (\partial u / \partial y), \quad (3)$$

and he then assumed mixing length to vary with the distance y from a wall as follows,

$$l = Ky = (0.40 \text{ or } 0.41)y \quad (4)$$

The successes of the Prandtl model - as evidenced over the decades - are essentially two-fold: It provides a conceptual basis for Equation (1) and it furnishes solutions for many practical turbulent flow problems. In short, it has compiled an excellent track record, as paraphrased by Coles

[5]. The ability of Prandtl's mixing length model in recovering the wall-law expression of Equation (1) suffers from one minor inconvenience: the intercept constant  $C$  in Equation (1) remains undetermined. Empirically, the velocity profile from the wall position  $y^+ = 0$  to where the turbulent "core" lies, say, at  $y^+ \approx 100$  is expressible by three segments: a sublayer region  $y^+ < 10$ , a buffer region  $10 < y^+ < 60$ , and a core region or wall-law region  $y^+ > 60$ . Each region may be described by a different, convenient algebraic expression.

The missing link unifying all three regions was supplied in 1956 by van Driest [6], who postulated a damping factor which modifies Prandtl's mixing length. His formulation is based on the concept that near a wall, the turbulent shear stress must be of a higher order of  $y$  than 2, as Equations (2) and (3) would indicate; and he proposed a damping factor on the mixing length as follows:

$$D = 1 - \exp(-y^+/A) \quad (5)$$

where a numerical value of 26 is recommended for  $A$ . Thus, calculation of the turbulent velocity distribution for a constant stress condition, referred to as Couette flow, can be carried out by using normalized (plus) coordinates through the following equations:

$$du^+/dy^+ = 1/[1 + \epsilon^+] \quad (6a)$$

$$\epsilon^+ = (\mu_t/\mu) \quad (6b)$$

$$\epsilon^+ = (l^+)^2 \left| du^+/dy^+ \right| \quad (6c)$$

$$l^+ = Ky^+[1 - \exp(-y^+/A)] \quad (6d)$$

The first one of the preceding equations, (6a), is for constant total shear - molecular plus turbulent - over the entire boundary layer thickness in which the Couette flow assumption is valid. The use of these equations permits a direct calculation of the velocities in three regions in one continuous stretch. However, two parallel, branch cases exist: in one, turbulent viscosity is considered a primary parameter to be postulated directly, and Equations (6c) and (6d) are not needed in this scheme; and in the other, mixing length  $l^+$  is postulated by Equation (6d) and all four equations of the group are involved. These two cases can be expressed by the following calculation equations:

$$du^+/dy^+ = 1/[1 + \epsilon^+] \quad (7)$$

and

$$du^+/dy^+ = 2/[1 + \sqrt{1 + 4l^{+2}}] \quad (8)$$

Following the mixing length postulate, van Driest [6] was able to show excellent agreement with experimental data over a wide range of  $y^+$  from 0 to 400, beyond which the law of the wall is no longer adhered to by experimental data. In the outer region where convective currents caused by entrainment from the main flow become influential, the velocity distributions were synthesized by Coles [7]; and from his analysis, he deduced the law of the wake - so named by Coles because the distributions are very much like that in a wake.

So far, the main elements in turbulent boundary layer analysis consist of Prandtl's mixing length, van Driest's damping factor and Coles' wake function description. To these basic building blocks there have been a number of significant extensions for flows with pressure gradients, mass transfer or transpiration at the wall, and streamwise curvature.

In parallel with these developments, other turbulence models have emerged; they were tailored for dealing with shear flows without a solid wall, such as jets and wakes. And the models proposed are primarily based on turbulent viscosity as a postulated parameter rather than mixing length. To avoid straying from the purpose of analyzing the rough-wall turbulent boundary layers, these phenomena will not be a part of the present work.

## II.2 Recent Modifications for Rough Surfaces

Based on an obvious observation that surface roughness promotes additional chaos in the flow, a simple modification is to postulate that the mixing length is increased by a factor  $R$ . Trying a new formulation like the following,

$$l = RKy \quad (9)$$

would satisfy the conceptual requirement as noted. However, the use of Equation (9) results in a wall-law expression which differs from Equation (1), in that it has a slope of  $1/RK$ . Experimental data on rough-surface boundary layer flows provide overwhelming evidence that the slope of the plus-coordinate plot,  $u^+$  versus the log of  $y^+$ , remains unchanged. Conceptually acceptable though, this approach is seen to lead to a

contradiction with the experimental data. Undoubtedly, this approach has been tried by many a researcher including the present author, only to be subsequently abandoned.

Apparently aware of the conflict, van Driest [6] in his widely noted paper in 1956 discussed and advanced an interesting idea to adapt his formulation to rough-wall boundary layers. Purely from a numerical viewpoint, the wall-law for a rough surface has the same slope as for a smooth surface but has a lower value for the intercept constant  $C$  or  $E$  in Equations (1), and this can come about if the mixing length  $l^+$  defined in Equation (6d) can be increased without affecting the slope upon reaching the wall-law region. To accomplish this, van Driest proposed and showed that his damping constant  $A$  can be made successively smaller as the roughness Reynolds number  $k_s^+$  increases. His calculated curves do exhibit the desired characteristic of lowered intercepts in the wall-law region and preserve the same slope as in the smooth-wall case. By comparing with experimental data, a relationship between his damping constant  $A$  and the roughness Reynolds number  $k_s^+$  was established from  $k_s^+ = 0$  up to a limit of 60, at which the damping constant  $A$  becomes zero. Beyond  $k_s^+$  of 60, van Driest's modification is, as he stated, not capable of describing the rough-wall velocity distributions.

Following this general outline, subsequent researchers sought to remedy this shortcoming. McDonald and Fish [8] adopted the idea of letting van Driest's damping factor exceed the value of 1. They did this by an additive term to the right-hand side of Equation (5) and stated that such a modification allowed calculations of the velocity distributions up to  $k_s^+ = 10^4$ . In an analogous manner, Healzer, Moffat and Kays [9] also undertook the modification task by allowing the damping constant  $A$  to

decline to zero as  $k_s^+$  increases from zero to 55; beyond this value, van Driest's damping factor is kept at unity, but the mixing length is increased by an amount  $\Delta l^+$  which depends on the overage ( $k_s^+ - 55$ ).

Differing from the preceding methods, Rotta [10] in 1962 proposed an idea of coordinate shift to accommodate the rough-wall velocity characteristics. His procedure, as shown by Cebeci and Smith [11], is identical to replacing  $y^+$  in Equation (6d) by  $(y^+ + \Delta y^+)$ , where  $\Delta y^+$  is a pre-determined coordinate shift and is dependent on  $k_s^+$ . Conceptually speaking, Rotta's idea recognizes the fact that at the tips of the surface protrusive elements, the velocity  $u^+$  represents a cumulative effect emanating from the deepest recesses of the surface asperities. According to this method, calculated results were presented by Momoh [12], who indicated that agreement with Nikuradse's sandgrain-roughened pipe data was good within 15 percent of each other. Part of the discrepancy may be attributed to the shift-method and part to the fact that adaptation of the Prandtl-van-Driest combination is still filled with loose ends for pipe flows.

And there is a fundamental inconsistency common to all the modifications enumerated so far: That the condition of  $du^+/dy^+ = 1$  at the wall  $y^+ = 0$  is not met, whether the method is a coordinate-shift by an amount of  $\Delta y^+$  or an incremental mixing length by an additional  $\Delta l^+$ , for then the mixing length value at  $y^+ = 0$  is no longer zero but finite. In finite-difference calculations without employing the so-called wall-function technique as a short cut, this deficiency may prove crucial.

### II.3 A New Formulation for Smooth Surfaces

To search for a remedy to account for the surface roughness influences

that can be used in concert with the finite-difference calculation scheme, it appears reasonable to accept Prandtl's postulate conceptually and qualitatively. Quantitatively the prescription need not be in the form of a linear function of  $Ky$ . First, the wall-law expression, Equation (1a), is cast into

$$y^+ = \exp(Ku^+)/E. \quad (10)$$

A set of commonly accepted constants for  $K$  and  $E$  are 0.4 and 9.025; the latter corresponds to a value of 5.5 for  $C$  in Equation (1). Equation (10), although it is a wall-law statement, can be interpreted to describe the mixing length variation  $l^+$  in terms of the velocity-coordinate  $u^+$ . Since at great distance from the wall,  $l^+$  is a linear function of  $y^+$ , with van Driest's damping factor nearly unity, the non-dimensional mixing length  $l^+$  can be alternately expressed by

$$l^+ = (K/E)\exp(Ku^+). \quad (11)$$

The use of Equation (11), in lieu of Equation (6d), and the condition of equal stress for Couette flow would lead to the law of the wall, but with an undefined integration constant which only a definite-integration step starting from the wall position  $y^+ = 0$  can produce. In the process of integrating starting from the wall, the mixing length variation defined by Equation (11), as the wall position is approached, must be examined. Since, on physical grounds,  $l$  must shrink to zero at the wall, where  $u^+ = 0$ , therefore the mixing length prescription by Equation (11) requires an additive term on its right-hand side which must be of no consequence at



large  $u^+$  but must make  $l^+$  zero at  $u^+ = 0$ . So, put  $l^+$  in the form

$$l^+ = (K/E)[\exp(Ku^+) - \exp(-Ku^+)] \quad (12a)$$

or, in another way,

$$l^+ = (K/E)\{\exp(Ku^+) - [1 + (Ku^+) + (Ku^+)^2/2]\} \quad (12b)$$

In the latter version, the added terms are obviously the first three terms of the expansion from the exponential member. As an alternative to mixing length being a primary turbulence quantity, turbulent viscosity may be considered as the first input, as a number of investigators have done in the past. Hence Equations (12a) and (12b) may be used to specify  $\epsilon^+$  in lieu of  $l^+$  on the left-hand sides of these two equations.

(In searching the literature pertaining to this type of modeling effort, it was noted that Spalding [13] in 1961 had proposed a unified expression for the velocity distribution from the wall up to wall-law region. His proposed expansion is:

$$y^+ = u^+ + \{\exp(Ku^+) - [1 + (Ku^+) + (Ku^+)^2/2 + (Ku^+)^3/6]\}/E. \quad (13)$$

And from it, he deduced an expression for turbulent viscosity  $\epsilon^+$ , very similar to Equation (12b), which was subsequently used by Kleinstein [14] in 1967 in his pipeflow analysis.)

To summarize, there are four proposed models, all quite similar in the general outline, for the calculation of turbulent velocity distributions. The four formulations can be used in conjunction with either Equation (7)

or (8). These four formulations are grouped below:

$$\begin{aligned}
 (i) \quad \epsilon^+ &= (\mu_t/\mu) = (K/E) \{ \exp(Ku^+) - [1 + (Ku^+) + (Ku^+)^2/2] \} \\
 (ii) \quad l^+ &= (l u_t/\nu) = (K/E) \{ \exp(Ku^+) - [1 + (Ku^+) + (Ku^+)^2/2] \} \\
 (iii) \quad \epsilon^+ &= (K/E) [ \exp(Ku^+) - \exp(-Ku^+) ] \\
 (iv) \quad l^+ &= (K/E) [ \exp(Ku^+) - \exp(-Ku^+) ].
 \end{aligned} \tag{14}$$

To test the ability of these formulations, (i) through (iv), in describing the  $u^+$  vs  $y^+$  variation for a smooth wall, each of these four forms was introduced into Equation (7) or (8) and integrated from  $y^+ = 0$  up to  $y^+ = 400$  approximately. In the numerical process, 0.40 and 8.134 were assigned to K and E respectively; the latter corresponds to an intercept constant of 5.24 for C in Equation (1) for the wall-law, i.e.

$$\begin{aligned}
 u^+ &= (\text{Log}_e y^+ + \text{Log}_e E)/K \\
 &= 2.5 \text{Log}_e y^+ + 5.24.
 \end{aligned} \tag{15}$$

The value of 8.134 for E was selected because in van Driest's analysis using his damping factor he reached the wall-law region with its velocity distribution given by Equation (15), and in this way the velocity distributions based on these four formulations can be compared with that of the commonly accepted van Driest's profile.

The resulting  $u^+$  vs.  $y^+$  variations are displayed in Figure 1. All curves bunch at the extremes of the transverse position ( $y^+ < 5$  and  $y^+ > 100$ ). For the intermediate position (buffer region), formulations (i) and (iv) and that of van Driest exhibit virtually indistinguishable patterns,

while formulations (ii) and (iii) show the greatest divergence from each other. The curve in Figure 1, based on formulation (i), corresponds to the closed-form expression,

$$y^+ = u^+ + (1/E) \left[ \exp(Ku^+) - [1 + (Ku^+) + (Ku^+)^2/2 + (Ku^+)^3/6] \right]. \quad (16)$$

Formulation (iii) yields an even simpler expression; namely,

$$y^+ = u^+ + (2/E) [\cosh(Ku^+) - 1]. \quad (17)$$

Its  $u^+$ -values are only slightly less than the accepted van Driest numerical results.

From these comparative results, as shown in Figure 1 for smooth walls, formulations (i) and (iv) seem to be superior to formulations (ii) and (iii).

A second comparison of this same group of formulations is presented in Figure 2, where for each case the wall-region velocity profiles have been evaluated using  $K = 0.40$  and  $E = 9.025$ . These constants were chosen in accord with Nikuradse's asymptotic smooth-wall equation

$$u^+ = 5.75 \log_{10} y^+ + 5.5. \quad (18)$$

Shown also in Figure 2 are experimental data transcribed from Eckert and Drake [15]. Again, comparative trends similar to Figure 1 are apparent; formulations (i) and (iv) give almost identical mid-region results.

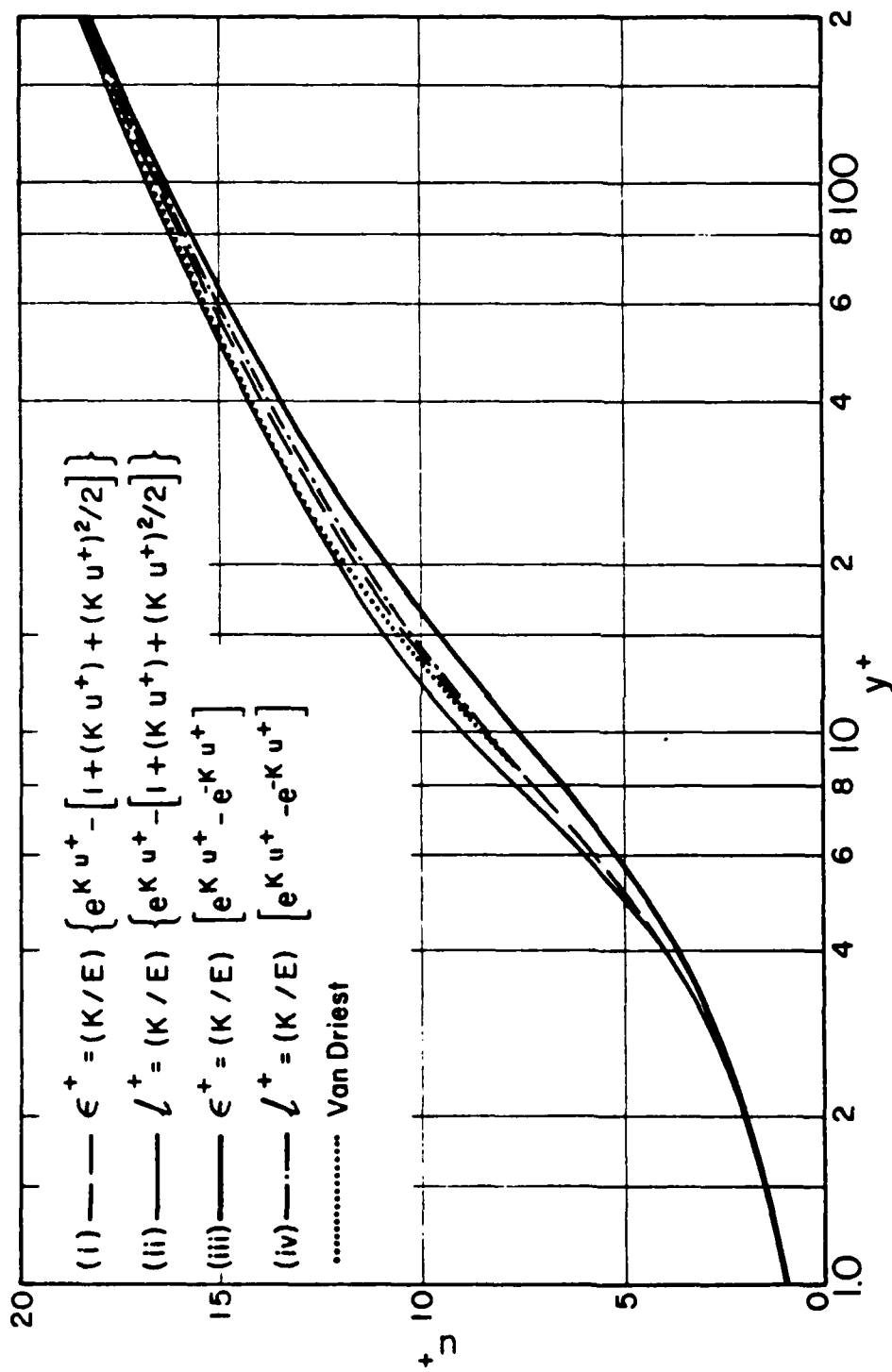


Figure 1 Comparative Velocity Profiles with Wall-Law

$$u^+ = 5.75 \log_{10} y^+ + 5.24 \quad (K = 0.4, \quad E = 8.134)$$

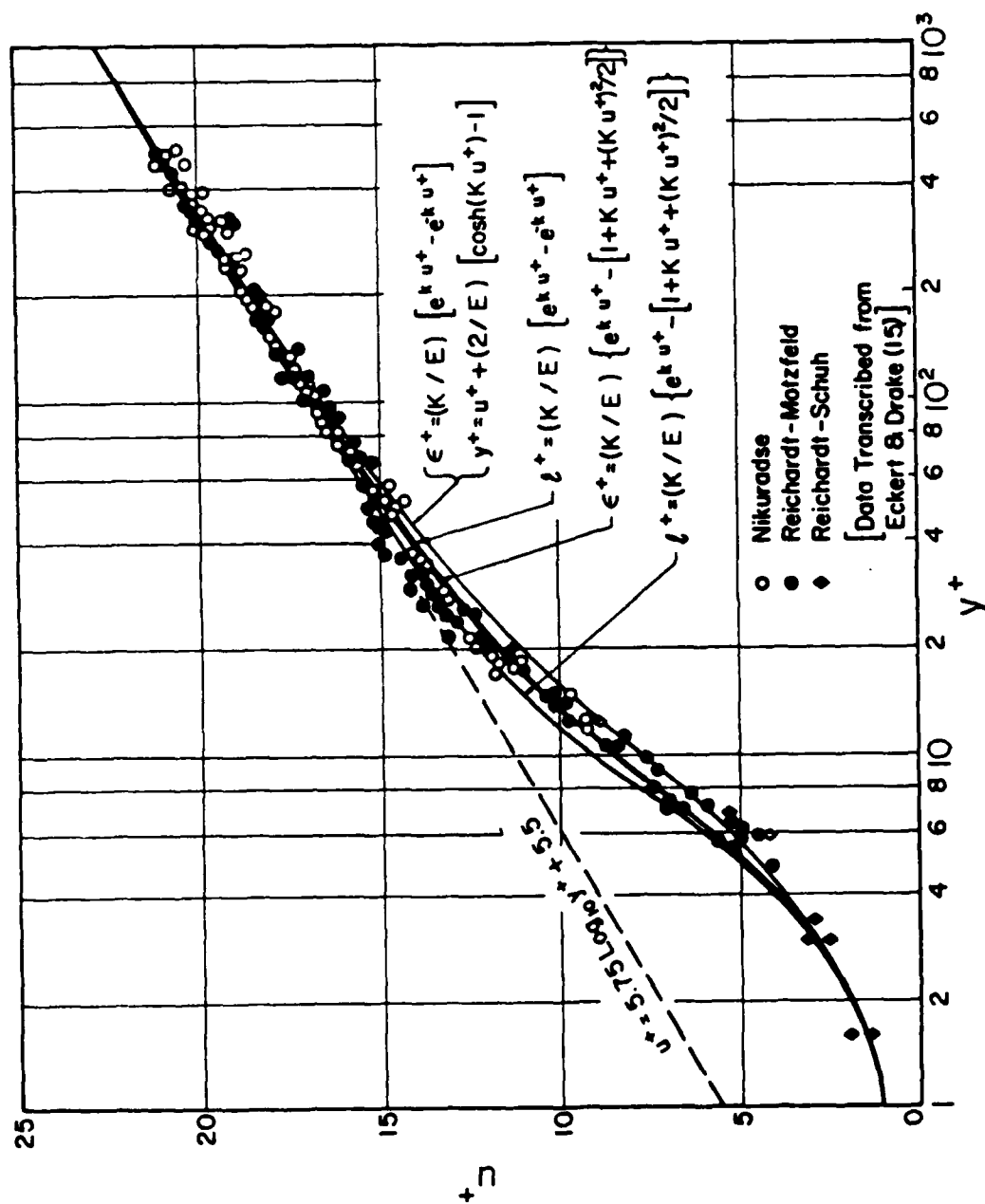


Figure 2 Comparison of Smooth-Surface Data with Various Formulations

#### II.4 Extension to Rough Surfaces

All of the four formulations, (i) through (iv) of equation (14), have one characteristic in common: at large values of  $u^+$  or what amounts to the same thing, where the wall-law is valid, the right-hand sides of these formulations become identical and are given by

$$\epsilon^+ \text{ or } l^+ = (K/E) \exp(K u^+), \quad (19)$$

which can be used in conjunction with the constant-stress condition of Couette flow to recover the law of the wall. It is of significance to note that the slope of  $u^+$  versus  $\log_e y^+$  is dictated by  $K$  inside the exponential term of Equation (19), and that the slope is unaffected by the proportionate coefficient  $(K/E)$ . It is this coefficient that provides an extra degree of freedom which can be used to account for the roughness influence in raising the mixing length or the turbulent viscosity.

Taking up this degree of flexibility, the mixing length  $l^+$  or turbulent viscosity  $\epsilon^+$  of formulations (i) through (iv) of Equation (14), valid for smooth surfaces, is multiplied by a factor  $R$  - called the amplification factor - to account for the increase owing to surface roughness. To illustrate this method of analysis and its ensuing results, the use of formulation (iii) will be considered. The rough-surface turbulent viscosity is represented by,

$$\epsilon^+ = R(K/E) [\exp(K u^+) - \exp(-K u^+)] \quad (20)$$

which, in conjunction with the assumption of a constant-shear stress [i.e.,  $(1 + \epsilon^+) (\partial u^+ / \partial y^+) = 1$ ], will lead to a velocity profile given by,

$$y^+ = u^+ + (2R/E)[\cosh(Ku^+) - 1]. \quad (21)$$

At large  $u^+$ , the above expression is asymptotically equivalent to

$$u^+ = [\log_e y^+ + \log_e E - \log_e R]/K. \quad (22)$$

This equation has the same slope of  $1/K$  as for smooth surfaces and its last term obviously represents the downward shift of  $u^+$  in the wall-region for which there exist ample data in the literature. The quantitative relation between  $R$  and  $\Delta u^+$ , the downward shift, is therefore,

$$\Delta u^+ = (1/K) \log_e R. \quad (23)$$

This relationship indicates that a large  $R$  results in a pronounced downward shift of  $u^+$ . This is in turn caused by a large roughness Reynolds number. These observations are in consonance with one another conceptually and mathematically.

While the foregoing analysis is based on formulation (iii), which has a very simple composition and is easily manipulated, the general outline remains unchanged, regardless of the formulation used in obtaining the velocity profile.

The preceding, simple algebra lends simplicity and a reasonable degree of completeness in the new modeling effort. The essential feature is that the roughness effect is directly expressed as an amplification factor  $R$  to either the mixing length or the turbulent viscosity, which are the newly developed expressions - formulations (i) through (iv) of Equation (14) in

terms of a velocity-space  $u^+$ , rather than Prandtl's algebraic expression in terms of  $y^+$ .

## II.5 Preferred Model Formulations

Although all four formulations (i) through (iv) of equation (14) give satisfactory accounting for the velocity distribution on a smooth surface from the laminar sublayer through the buffer region to the turbulent core, it is desirable, however, to establish a choice by examining their relative merits. A primary criterion is, naturally, how well results based on these model formulations compare with the available experimental data and other established analytical deductions. For flow over smooth surfaces, the velocity distributions shown in Figures 1 and 2 indicate little difference for  $y^+ < 10$  and for  $y^+ > 100$ ; and only in the buffer region, where  $y^+$  varies from 10 to 100, are the results different from one another, and only mildly so. For rough surfaces, the difference between results from these model formulations is expected to grow, and thereby provides a further criterion for differentiation.

For this purpose, the only data found which give experimental determined values of  $u^+$  vs.  $y^+$  for rough walls are in Robertson's work [16]. He measured the velocity distributions near sand-roughened pipe walls from  $y^+ = 10$  to the fully developed eddy-region for different surface roughnesses. The measured velocity deficit  $\Delta u^+$  is in reference to the smooth-surface wall-law of the form

$$u^+ = 5.6 \log_{10} y^+ + 5.6 \quad (24)$$



which was also recommended by Ross [17] after a thorough, critical study of Nikuradse' data to re-define the wall-law constants. The numerical values used in Equation (24), which correspond to  $K = 0.411$  and  $E = 10$ , were obtained by comparing Equation (24) with Equation (1a).

Robertson's data (shown in Figure 10 of his paper) are divided into several sets, each of which is characterized by the downshift  $\Delta u^+$  - the difference between the rough surface wall-law and the smooth-surface wall-law of Equation (24). Thus, for each set of  $u^+$  vs.  $y^+$  measurements, the measured asymptotic downshift  $\Delta u^+$  is used to calculate the amplification factor  $R$  through equation (23). With  $K$ ,  $E$  and  $R$  determined, formulations (i), (iii), and (iv) are used in conjunction with either Equation (7) or (8) to generate the velocity distribution curves, which are shown in Figures 3, 4, and 5 respectively. From formulation (i) of Equation (14), the computed curves, shown in Figure 3, indicated greatest divergence from his experimental values; this formulation along with formulation (ii) are therefore not further taken up. The other two models, formulations (iii) and (iv), whose results are shown in Figures 4 and 5, show very good agreement with Robertson's data. Model (iii) based on the turbulent viscosity  $\epsilon^+$  has an added attraction: that a simple relation exists between  $u^+$  and  $y^+$ , i.e. Equation (21).

Model (iv) based on the mixing length is the preferred formulation, for in the boundary layer analysis mixing length is viewed as more primary than turbulent viscosity.

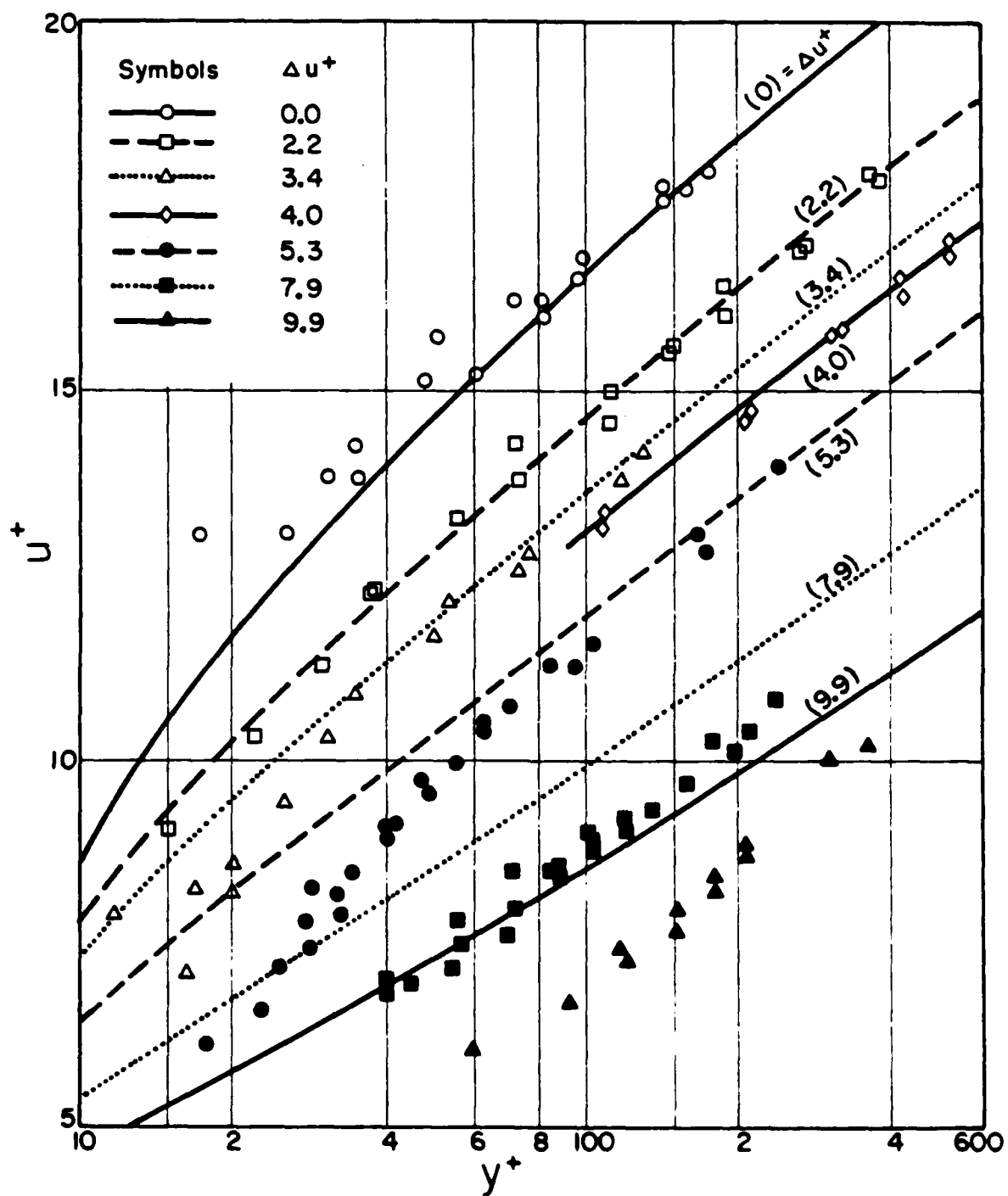


Figure 3 Comparison of Robertson's Data with Calculated Profiles, Model for Turbulent Viscosity (1)

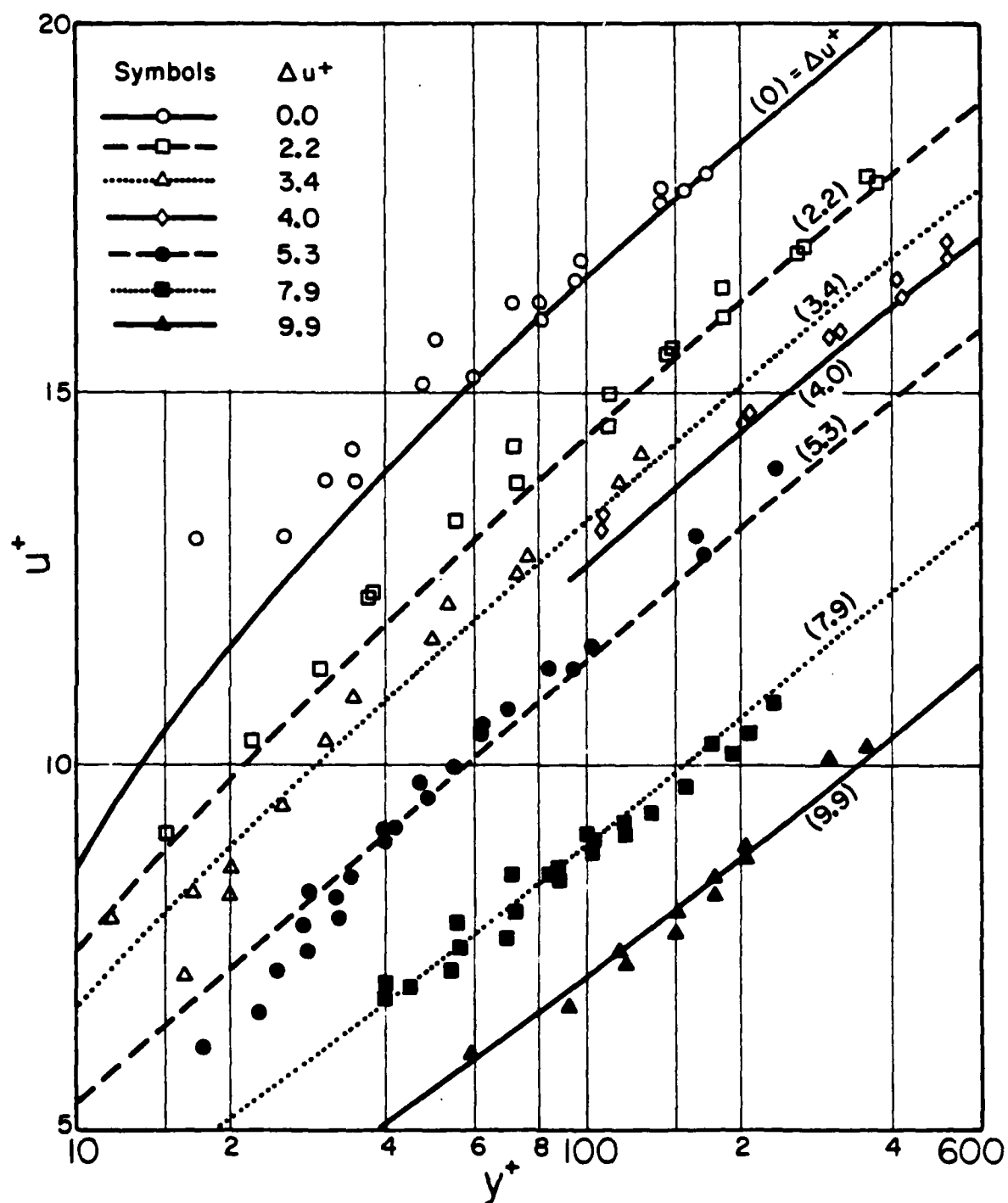


Figure 4 Comparison of Robertson's Data with Calculated Profiles, Model for Turbulent Viscosity (111)

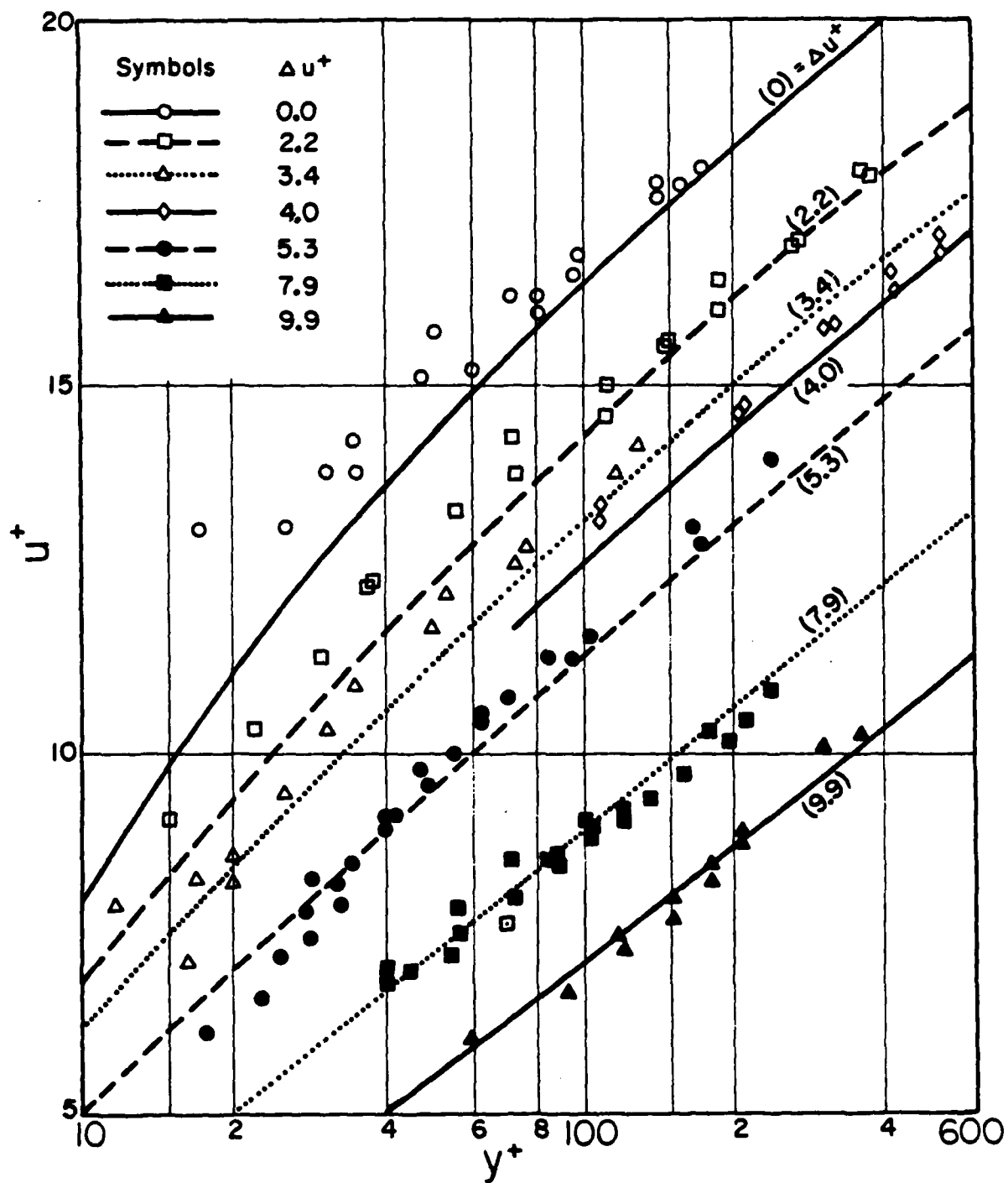


Figure 5 Comparison of Robertson's Data with Calculated Profiles, Model for Mixing Length (iv)

### III. THE ROUGHNESS AMPLIFICATION FACTOR

Having demonstrated that the model formulations in Equation (14) - particularly, formulation (iv) for mixing length - are viable turbulence models for flow over smooth and rough surfaces, all that is needed to complete the methodology is a quantitative relation between the surface roughness ~~size~~ and the factor of amplification. This relation can only come through experiments.

Since surface roughness and mixing length amplification are local phenomena in the vicinity of the surface protrusions, the flow in the immediate neighborhood of a rough wall may be likened to a flow over a sphere.

The protrusive roughness is equivalent to a sphere radius and the friction velocity  $u_t$  is of the same order of the freestream velocity for a single sphere. Thus, the nondimensional roughness factor  $k_s^+ = (k_s u_t / \nu)$  is equivalent to the Reynolds number for flow over a sphere. For low Reynolds numbers, the flow pattern is that of a creeping laminar flow without separation in the rear of the sphere. In this regime of flow, the corresponding phenomenon in the rough-wall turbulent boundary layer is complete immersion of the wall protrusions in the laminar sublayer.

With increasingly higher Reynolds numbers, leeward separation of flow is manifested in the second-order effect (inertia) of drag. Eventually, separation bubbles are transformed into continuous vortex shedding; its frequency and scale are determined by a linear function of the flow Reynolds number  $k_s^+$ . The latter observations are in qualitative agreement with the experimental findings for a single sphere. Translated to the

rough-wall boundary layer, the mixing length  $l$  or eddy viscosity  $\mu_t$  can be considered linearly dependent on the protrusion scale.

For a rough surface comprised of protrusions of various sizes, the vortex-wake would be more of a continuous event with vortex shedding first from the larger roughness elements and then from the smaller elements as the friction velocity  $u_t$  increases. When the protrusions are of the same size, the vortex-wake would likely exhibit a phenomenon of nearly simultaneous onset, preceded by a period of inertness.

Keeping in mind the above described qualitative events, attention is turned to the quantitative aspect of the amplification factor. In general, the amplification factor must be dependent on the physical size of the roughness elements protruding from a surface; on the pattern of distribution, whether random or uniform in size; on their physical description, grooves, two or three-dimensional in their dispersion; and of course on their spatial scatter on the surface. These four factors, as comprehensive as they can be made, exert varying degrees of influence on turbulent mixing near the surface. In a thorough analysis and survey of the rough-surface data, Lakshman and Jayatilleke [18], following the approach of Spalding, reported a large number of experimental data of the velocity deficit  $\Delta u^+$  in the wall-law region. There is also a large body of literature pertaining to the influence on heat transfer of surface roughness, usually expressed in terms of an augmentation factor caused by a particular kind of roughness element, such as ribs, spirals, etc. Not all of the data mentioned are, however, amenable to a fundamental synthesis with the purpose to extract amplification factor  $R$  from these sources.

In favor of essentials rather than comprehensive coverage at this stage, attention is focused on the most well-acknowledged rough-surface

experimental data. First and foremost is the data set of Nikuradse' pipeflow experiments. His results as well as his analysis of them are presented by Schlichting [13], but in greater details by Bakhmeteff [1]. Next follows the work of Moody [2], whose compendium on random distributions of manufacture-originated commercial roughness in pipeflow is, as mentioned before, a widely used reference. In addition, the data of Colebrook-White [19] and Hama [20] are sufficiently complete to permit the establishment of the amplification-versus-roughness relations for the types of roughness treated by them. The choice of these four sources is predicated by the completeness of the data for the purpose of synthesis, and though few in number, they do span two representative classes. One class of data - Nikuradse' and Hama - belongs to the category of uniform size, and the other - Colebrook-White and Moody's - represents randomness in distribution.

### III.1 Amplification Factors for Nikuradse' Sandgrain Roughnesses

Nikuradse' pipeflow data are widely recognized as an indispensable source of information which ultimately led to the empirical and phenomenological formulation of turbulent boundary layer analysis as it presently stands. Although re-examined by Ross [17] in the early fifties for the purpose of repairing some minor inconsistencies in the data treatment, the originally measured pipeflow resistance coefficients and others remain, however, undisputed. In the near-wall region, Nikuradse' data were expressed by him in a logarithmic equation,

$$u^+ = 5.75 \log_{10} y^+ + 5.5, \quad (25)$$

in which the coefficients correspond to  $K = 0.4$  and  $E = 9.025$ . Ross' re-examination and re-analysis of Nikuradse' data resulted in equation (24), which differs from Equation (25) only very insignificantly. At  $y^+ = 10^4$ , for example, the values produced by these two equations are 28.0 and 28.5, respectively.

For flow inside rough pipes, Nikuradse used the wall-law formula, like Equation (25), but with a velocity deficit  $\Delta u^+$  in the right-hand side of the equation. He then proceeded to determine  $\Delta u^+$ , primarily based on his measured friction coefficients in rough pipes.

Nikuradse' Procedure for Intercept Constant B. In his analysis of the rough-pipe data, Nikuradse assumed that the wall-law expression, equation (25), or its equivalent for a rough-wall, is valid for the entire pipe, an assumption no longer accepted because there are now more reliable profile data to show otherwise. Based on this assumption, Nikuradse integrated Equation (25) across the entire pipe to obtain an average velocity  $u_a$ . The resulting formulation contains the average velocity of the flow and the friction velocity at the wall  $u_\tau$ ; with minor adjustments to the numerical coefficients, a formula for determining the flow resistance coefficient  $f$  in smooth pipes is obtained by him as follows,

$$1/\sqrt{f} = 2 \log_{10} (Re \sqrt{f}) - 0.8 \quad (26)$$

which is in excellent agreement with his experimental data.

For flow in rough pipes, a similar procedure was followed. It commenced with a wall-law Equation (1) but with an intercept constant  $C$  undefined. Again assuming its validity for the entire pipe cross-section,



a formula relating the pipe Reynolds number and the pipe friction coefficient  $f$  was obtained. As the pipe friction coefficient  $f$  was known through experiments, the value for the intercept constant  $C$  in the wall-law Equation (1) was then determined in this inverse fashion.

Instead of using the intercept constant  $C$  directly, Nikuradse expressed his results by defining an intercept function  $B$  through the following equation:

$$u^+ = (\text{Log}_e y^+ - \text{Log}_e k_s^+) / K + B \quad (27)$$

where 0.4 is used for  $K$ , and  $k_s^+$  is the roughness Reynolds number. Equation (27) is a general representation for the wall-law for  $k_s^+ = 0$  to  $\infty$ , from smooth surface to surfaces with "full roughnesses". The latter region is characterized by such strong turbulence mixing caused by surface protrusions that molecular viscosity is of no consequence in affecting the velocity distribution in the Couette-flow zone. In this event,  $B$  in Equation (27) tends to a numerical constant, thus cancelling the presence of the molecular viscosity in  $y^+$  and  $k_s^+$  from the equation.

In the other extreme, as the surface roughness diminishes in size, i.e.  $k_s^+ \rightarrow 0$ , then Equation (27) should revert itself to Equation (25), and the  $B$ -function should become asymptotically,

$$B = 5.5 + 5.75 \text{Log}_{10} k_s^+ \quad (28)$$

as  $k_s^+ \rightarrow 0$ .

The numerical values for  $B$  as determined by Nikuradse using the wall-law for the entire pipe cross-section are shown as symbols in Figure

6. The value of B becomes a constant of 8.48 at large values of  $k_s^+$ , and approaches the straight line representing Equation (28), for small values of  $k_s^+$ . The velocity downshift or deficit  $\Delta u^+$  is simply the difference between the B-value and the straight-line value of B, defined in Equation (28) for smooth surfaces. Thus for fully rough surface, i.e.  $k_s^+ \rightarrow \infty$  (in reality,  $k_s^+ > 100$ ),  $B = 8.48$ ; hence the velocity shift  $u^+$  can be put as

$$\begin{aligned} u^+ &= (5.5 + 5.75 \log_{10} k_s^+) - 8.48 \\ &= 2.5 \log_e k_s^+ - 2.98, \end{aligned} \quad (29)$$

which, when combined with Equation (23), gives a simple relation between the amplification R and the roughness Reynolds number  $k_s^+$  as

$$R = 0.3036 k_s^+ \quad (30)$$

for  $k_s^+ > 100$ .

For other  $k_s^+$ , their corresponding B-function values, represented by the symbol points or a mean curve through them, can be used to calculate  $\Delta u^+$  and hence R.

So in principle, the data in Figure 6, shown as symbol points, complete the analysis of Nikuradse' rough pipe flow resistance coefficients. However, while the experimentally determined pipe friction coefficients remain undisputed, there is room for improvement insofar as the assumption of the wall-law velocity distribution for the entire pipe cross-section is concerned. In order to confirm or refine the results from

Nikuradse' work, the process of extracting the amplification factor is re-examined in the next section.

The B-Function Re-Analyzed. Among the steps used to deduce the velocity deficit function, or B-function in Equation (27), it appears reasonable to take issue with regard to Nikuradse' use of the logarithmic profile for the entire pipe cross-section. No doubt, it was an expedient thing to do and had led to qualitatively acceptable results. However, in the interest of re-affirmation and refinement, this particular step is re-done here using the formulation adopted in this research, and taking into consideration the shear profile across the pipe cross-section. Starting with these premises, the velocity distribution in a round pipe is governed by,

$$[1 + (l^+)^2(du^+/dy^+)](du^+/dy^+) = [1 - (y^+/r_o^+)] \quad (31)$$

where  $r_o^+$  is the dimensionless pipe radius in the plus-coordinates, and  $y^+$  is the distance from the pipe wall. The dimensionless mixing length  $l^+$  is that of formulation (iv) of Equation (14) with an amplification factor R, or specifically given by

$$l^+ = R(K/E)[\exp(Ku^+) - \exp(-Ku^+)] \quad (32)$$

To be consistent with the coefficients used by Nikuradse, values of 0.4 and 9.025 are assigned to K and E respectively.

Use of Equations (31) and (32) for a smooth pipe, i.e.  $R = 1$ , did not result in satisfactory agreement between the calculated friction

coefficients and their experimental counterparts, but in a discrepancy of about 20 percent between the two. The same degree of disparity was also encountered by Momoh [12], as mentioned earlier. As often as pipe-flow velocity distributions have been analyzed, there is apparently no complete agreement among various investigators as to which model or method achieves the best results. Kleinstein [14], in his analysis of turbulent flow in pipes,, using a model formulation similar to one of the formulations of Equation (14), found it necessary to introduce a damping factor, linear in  $y$  and vanishing at the pipe axis, in order to bring about a satisfactory accounting between his analysis and the empirical results. Pipe flows with invariant profiles along the axial direction are essentially different from boundary layer flows in that the former case has a non-zero pressure gradient and no uniform external flow as an entrainment source while the latter possesses both. After a number of exploratory attempts, it is also found necessary to introduce into the mixing length expression a van Driest damping factor in order to achieve excellent agreement between the calculated and empirical friction coefficients.

Operationally, the process starts with an arbitrarily selected value for  $r_o^+$ , generally between 200 and  $10^5$ , into which  $y^+$  is divided into approximately 300 intervals, with  $y^+ = 0$  at the pipe wall and  $y^+ = r_o^+$  at the pipe axis. The integration steps near the wall are kept small with  $\Delta y^+$  less than 0.2 to accommodate steep gradients occurring there. Beginning with the condition  $u^+ = 0$  and  $y^+ = 0$ , Equation (31), in which  $l^+$  is defined by equation (32) with  $R = 1$  and modified by the van Driest damping factor, is integrated step-wise to obtain the  $u^+$ -distribution up to  $y^+ = r_o^+$ . The averaged  $u^+$  over the pipe cross-section gives the pipe friction coefficient  $f$  as follows:

$$u_a^+ = u_a/u_t = \sqrt{8/f} \quad (33)$$

where  $f$  is Darcy's pipe resistance coefficient. Simultaneously, a pipe flow Reynolds number (diameter based) is extracted from the  $r_o^+$ -value selected in the beginning of the procedure, i.e.

$$r_o^+ = (Re/2)\sqrt{f/8} \quad (34)$$

By assigning a range of values to  $r_o^+$ , pipe friction coefficients  $f$  are obtained for pipe Reynolds numbers from 6000 to  $10^6$ . The calculated results are shown as circle-points in Figure 7, which coincide with Nikuradse's smooth-pipe curve almost perfectly for  $Re$  greater than  $10^4$ .

Friction Factors for Rough Pipes. For rough pipes, the essential steps remain unchanged. Since the experimental data of Nikuradse are for a range of pipe roughness ratios in terms of  $(k_s/r_o)$ , the latter is needed for commencing the numerical procedure. Hence, for each numerical "run", a pipe roughness ratio, say,  $1/16$ , is fixed, in addition to an arbitrary value for  $r_o^+$ . As to the amplification factor  $R$ , its value is first taken from Nikuradse's  $B$ -function shown in Figure 6, corresponding to  $k_s^+$  computed by taking the product of  $(k_s/r_o)$  and  $r_o^+$ , both fixed in each integration process. The approximate value for  $B$  taken from Nikuradse's analysis as a first guess is used to calculate  $\Delta u^+$  and then the amplification  $R$ . The calculated friction factors  $f$  are then compared with Nikuradse's measurements for a series of pipe Reynolds numbers at a chosen pipe roughness factor. Discrepancy between the two is minimized by adjusting the velocity deficit  $\Delta u^+$  until satisfactory agreement is reached.

Essentially the above steps are intended to refine Nikuradse' B-function, which are obtained by the use of the logarithmic formulas for the entire pipe cross-section. For the pipe roughness ratios covered by Nikuradse, the calculated results thus refined are shown in Figure 7 together with the symbol-points of Nikuradse. The revised B-function is shown in Figure 6 and lies below those of Nikuradse' analysis, however only slightly. The minor shift confirms the qualitatively correct nature of Nikuradse' work. From the re-analyzed B-function, shown in Figure 6 as a solid curve, a set of amplification factors  $R$  for a range of  $k_s^+$  is obtained. They are shown graphically in Figures 8a and 8b and tabulated in Table 1.

### III.2 Other Types of Roughnesses: Moody, Colebrook-White and Hama

Unlike the roughnesses obtained by coating uniform sandgrains to the pipe surfaces in Nikuradse' tests, the data analyzed by the other investigators are for different textures. Moody's well-known treatment of commercial pipes of various kinds is in reality a collection of random-oriented roughness elements caused by the manufacturing processes, erosion, aging, etc. It is therefore expected that the amplification factors associated with his randomly oriented roughness protrusions would exhibit some fundamental differences.

Using basically the same procedure for Nikuradse' sandgrain roughnesses - specifically, taking Nikuradse' B-function as a first approximation to compute  $\Delta u^+$  and  $R$  - the resulting  $f$  vs  $Re$  relation for each pipe roughness factor,  $(k_s/r_0)$ , is compared with Moody's summary correlation. Successive attempts improve the corresponding B-function until acceptable pipe friction coefficients in reasonable agreement with

each empirical curve are obtained. Calculated friction factors for each pipe roughness ratio are shown in Figure 9 as symbols superimposed on each curve compiled by Moody. Conjugate to the friction factors, the B-function associated with Moody's random roughness parameter  $k_s^+$  is shown in Figure 6 as a dashed curve which lies appreciably below that for Nikuradse' sandgrain roughnesses but approaches the same plateau as the roughness Reynolds number increases. In addition, the computed amplification factor  $R$  as a function of  $k_s^+$  is shown graphically in Figures 8a and 8b and tabulated in Table 1.

Two additional types of surface roughnesses are included in this presentation: one that is produced by wirecreens studied by Hama [20] and the other is by Colebrook-White [19], who used sandgrains of mixed sizes to coat the surfaces. The former type is a manufactured roughness and is therefore considered uniform in texture; the latter, because of the mixed sizes, is considered nearly random. Colebrook-White's data are listed by Robertson [16] and Hama's wirecreen data are taken directly from his paper. Since the downshift velocities  $\Delta u^+$  are directly available at various values of  $k_s^+$ , their conversion into amplification factor  $R$  is a simple computation based on Equation (23) in which von Karman's constant  $K$  is 0.411, as used by the investigators themselves. The computed curves for  $R$  are shown in Figures 8a for low values of  $k_s^+$  and Figure 8b for high values.

Of these four roughness types treated in this investigation, Nikuradse' sandgrains and Hama's wirecreens belong to the category of uniform texture, and the other types - Colebrook-White and Moody's - are characterized by randomness of the roughness distribution in size. That the amplification curves for  $R$  due to the latter two types are close approximations to each other, as is evidenced in Figures 8a and 8b, is

a testimony to their random texture. Similarity between Nikuradse's sandgrain data and Hama's wirescreen curve shown in Figure (8a), especially in the low range of  $k_s^+ < 10$ , is underscored by the same shape of the distributions of  $R$  versus  $k_s^+$ . These two curves for uniform roughnesses exhibit a slow rising  $R$  at first and then assume a linear rise with  $k_s^+$  at large values of the latter. On the other hand, the shapes of the  $R$ - $k_s^+$  curves for Moody's and Colebrook-White's random roughness take on a linear shape at the very beginning of the amplification process.

These two contrasting variations may be reconciled by two vortex shedding phenomena associated with a surface containing protrusions of the same size and another containing protrusions of various heights, i.e. random. Thus, phenomenologically the variations of  $R$  vs  $k_s^+$  shown in Figures 8a and 8b reflect qualitatively the mechanisms with which turbulent mixing is enhanced progressively and sequentially by the roughness elements of various sizes situated on a same surface. Customarily, for uniform surface roughnesses, the influence is divided into three regions as follows:

- |                           |                  |
|---------------------------|------------------|
| (i) hydraulically smooth, | $k_s^+ < 5$      |
| (ii) transition,          | $70 > k_s^+ > 5$ |
| (iii) fully rough,        | $k_s^+ > 70$     |

From a vortex-shedding viewpoint, these three regions may also be called (i) dormant region, (ii) burst region, and (iii) continual-shedding region; these descriptions are self-explanatory. For random roughnesses, however, the first two regions no longer exist, judging from the amplification curves so compiled in Figure 8a .



In the full-rough region, data on  $R$  computed in this analysis yield a linear relationship to the roughness Reynolds number  $k_s^+$ . For uniform roughnesses of Nikuradse' sandgrain type, the full-rough region appears to start from  $k_s^+ = 100$  and for commercial random roughnesses of Moody's compendium, the region commences at  $k_s^+ = 600$ , though such a demarkation is a matter of judgement. Beyond these threshold values, the relationships can be put as

$$R = 0.3036 k_s^+ \quad (35)$$

for uniform sandgrain roughnesses and for  $k_s^+ > 100$ ; and

$$R = 0.2950 k_s^+ \quad (36)$$

for commercial random roughnesses and for  $k_s^+ > 600$ . For the other two types, their asymptotic relations are:

$$R = 0.327 k_s^+ \quad (k_s^+ > 40, \text{ Colebrook-White}) \quad (37)$$

$$R = 0.586 k_s^+ \quad (k_s^+ > 30, \text{ Hama}) \quad (38)$$

That these four different types of roughnesses exhibiting different amplifications in the full-rough region can be ascribed to a number of factors yet unexplored. One of these is the spatial distribution density of the roughness elements; still another is the intrinsic nature of the protrusions, i.e. shapes and the two or three dimensionality of the dispersed pattern. In this phase of work, attention is focused on the

establishment of the basic methodology and the factors just described will be relegated to the next phase of the overall investigation.

### III.3 Spatial Distributions of Velocity and Amplification Ratio

Computed Velocity Profiles. To round up the development, performance features of the methodology are presented in this section. First, the velocity profiles are computed for Couette flow across the entire boundary layer from  $y^+ = 0$  to  $y^+ = 200$ , where the wall-law starts to take over. The roughness Reynolds number  $k_s^+$  varies from zero for a smooth surface to 400, a value well over the mathematical limit of van Driest's modification method.

Two turbulence models are employed; one is based on mixing length formulation (iv) of Equation (14) and the other on viscosity formulation (iii). Each expression is multiplied by an amplification  $R$  which depends, of course, on the surface roughness Reynolds number and the type in question. These two model equations are repeated below:

$$\epsilon^+ = R(K/E)[\exp(Ku^+) - \exp(-Ku^+)] \quad (39)$$

$$l^+ = R(K/E)[\exp(Ku^+) - \exp(-Ku^+)] \quad (40)$$

Each of these equations is used in conjunction with either Equation (7) or (8) to compute the velocity profiles, and Colebrook-White's random roughness is taken to relate  $k_s^+$  with  $R$  needed in the model Equations (39) and (40). For the wall-law constants  $K$  and  $E$ , 0.4 and 9.025 are used.

Computed velocity profiles are shown in Figure 10 and the curves according to these two model Equations (39) and (40) are in close proximity to one another; in fact, from a numerical viewpoint it is difficult to favor one model against another. Features consistent with experimental data are apparent in these velocity presentations: namely that in the wall-region  $y^+ > 100$ , all curves are parallel with the same slope of  $1/0.4$  and that in the vicinity of the wall  $y^+ = 0$ , the condition of  $du^+/dy^+ = 1$  is observed. Furthermore, the viscous sublayer thickness is reduced as the roughness is increased; for a smooth surface, the sublayer extends to  $y^+ = 5$  and for  $k_s^+ = 400$  the layer is estimated to  $y^+ = 0.5$ . This is of course in consonance with the concept of increased mixing due to surface roughness.

Amplification Factor Distribution. The second performance feature of the methodology pertains to the amplification factor  $R$ . It is recalled that the amplification  $R$ , as shown in Equation (40), is a multiplier constant to the smooth-surface mixing length when expressed in the  $u^+$ -coordinate. If the numerical values of  $R$  were plotted against the various  $u^+$ -values across the boundary layer,  $R$  would appear as a flat, horizontal line. Such a presentation would reveal nothing insofar as its spatial variation is concerned. A meaningful question, on the other hand, is as follows: Assuming that for rough-wall boundary layers, the velocity distributions are to be calculated using Prandtl-van-Driest's prescription multiplied by a yet undetermined  $y^+$ -dependent augmentation factor, what kind of function of  $y^+$  should it be so that the resulting velocity profiles are those shown in Figure 10? Strictly speaking, the augmentation factor thus defined is not the ratio of the two physical mixing lengths - one for

a rough surface and the other for a smooth surface, for the scale factor involves  $u_t$  which are different for these two comparing references.

Since for a smooth surface, the velocity profile obtained by using Equation (40) with  $R = 1$  is not different from that resulting from the Prandtl-van-Driest combination, the augmentation factor can be obtained on the basis of the plus-coordinates. Operationally, the rough-wall mixing length  $l^+$  can be calculated from Equation (40) with an  $R$ -value of, say, 25.92, for which the velocity distribution is shown in Figure 10 at various  $y^+$ -values. Correspondingly, the smooth-wall mixing length  $l^+$  can be obtained by using the same Equation (40) but with  $R = 1$ . The ratio of the two dimensionless mixing lengths therefore varies with  $y^+$ . Thus for each  $R$ -value or  $k_s^+$ -value, there is a spatial distribution of the ratio that is shown in Figure 11. Near the wall or in the sublayer region, the ratio assumes the  $k_s^+$ -dependent  $R$ -value associated with the  $u^+$ -dependent model Equation (40). The ratio diminishes towards unity as  $y^+$  is increased. Mechanistically, the ratio may be interpreted as a local augmentation which is damped out in the outer region of the boundary layer. Or, mathematically, it is the shape of the function that needs to be multiplied to the Prandtl-van-Driest formulation in order to arrive at the profiles of Figure 10.

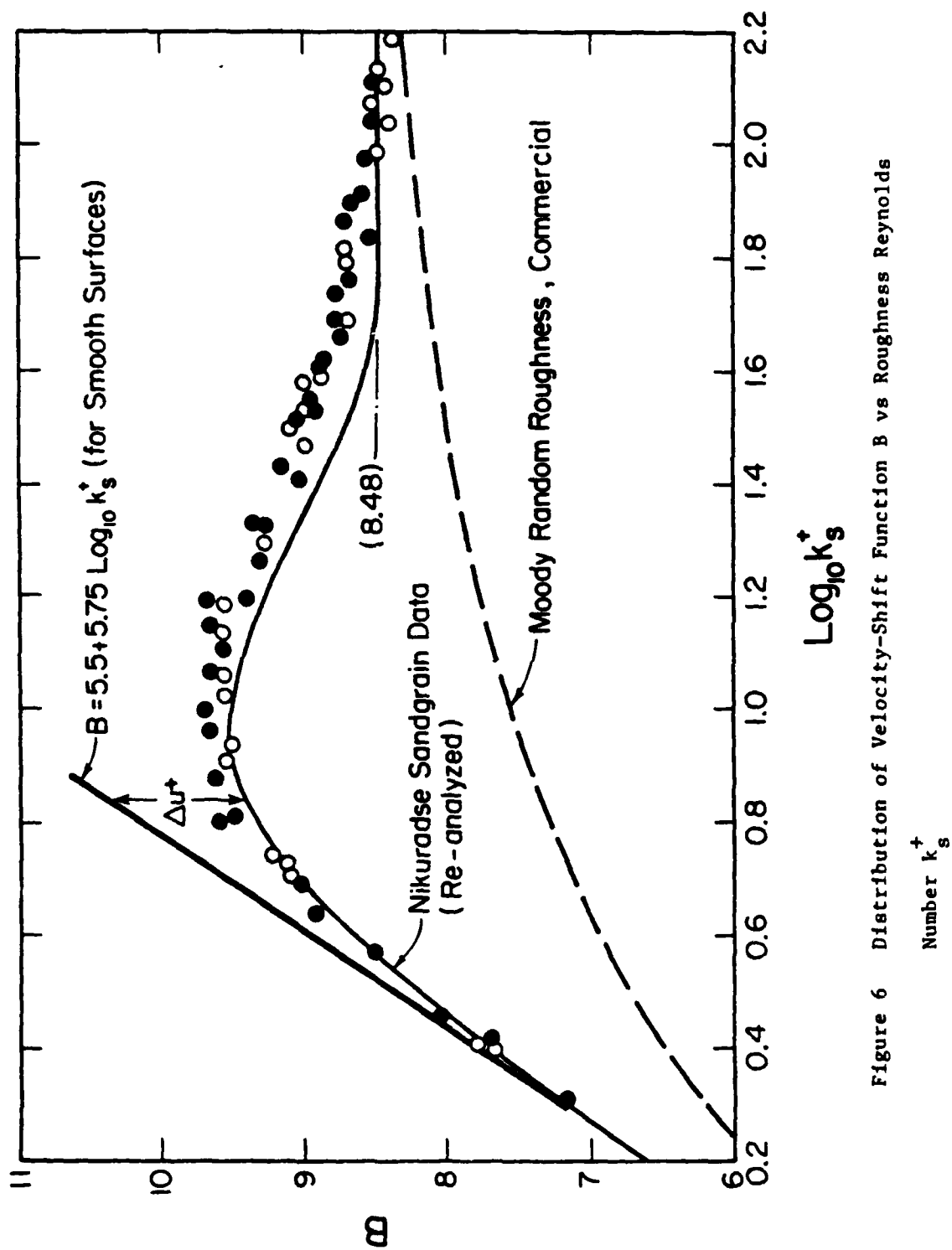


Figure 6 Distribution of Velocity-Shift Function B vs Roughness Reynolds

Number  $k_s^+$

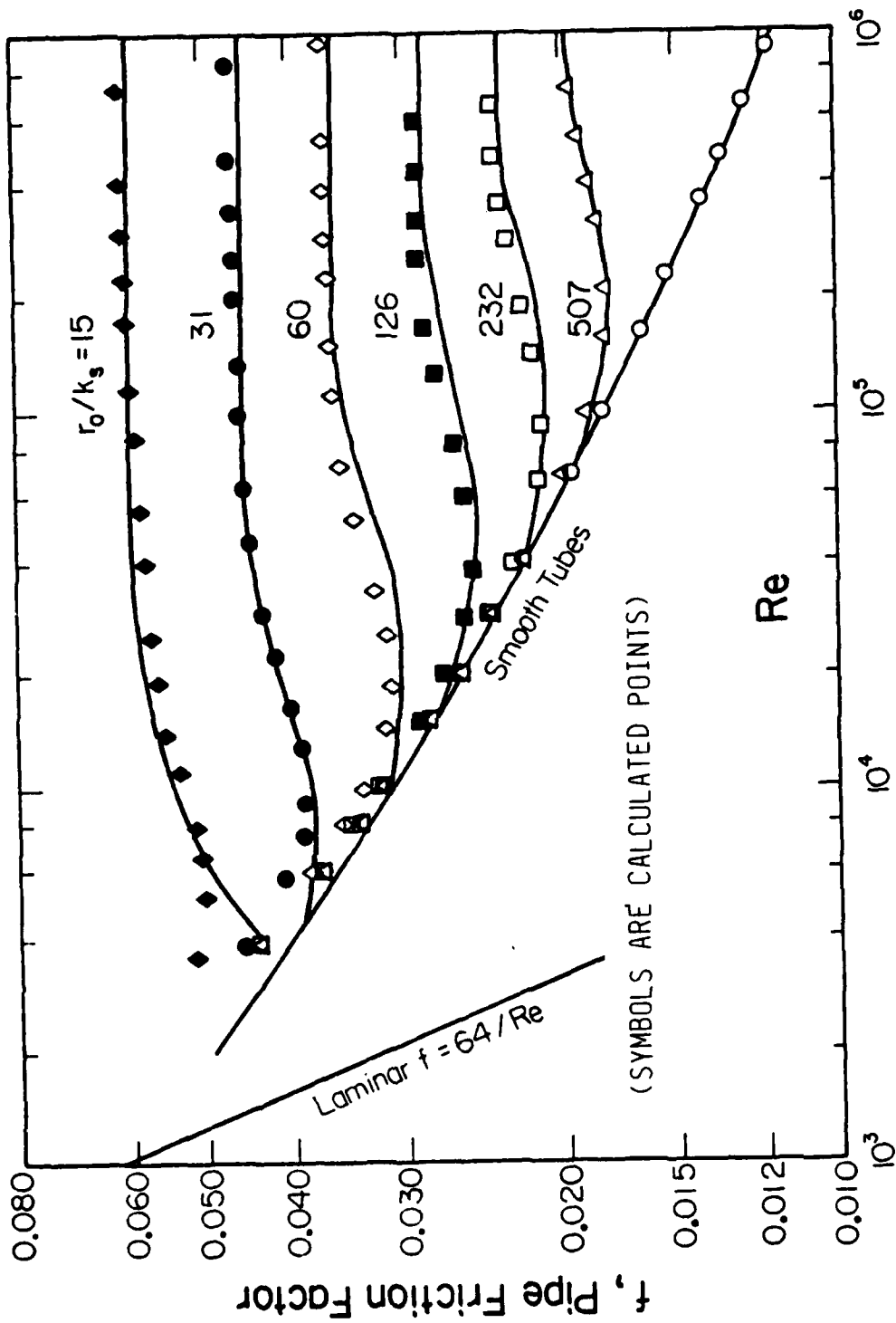


Figure 7 Calculated Pipe Friction Factors for Nikuradse' Sandgrain

Roughnesses

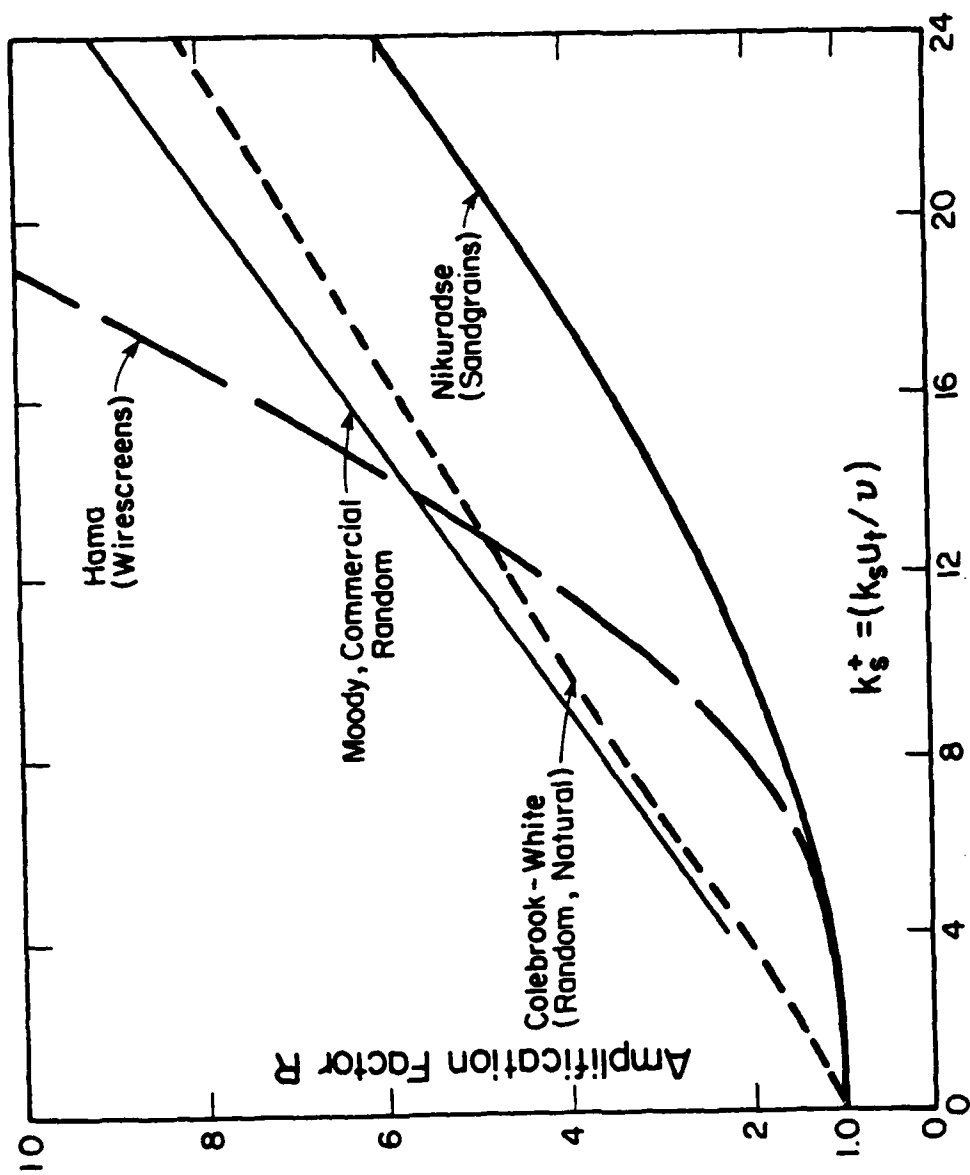


Figure 8a Mixing Length Amplification vs. Surface Roughness, Low Range

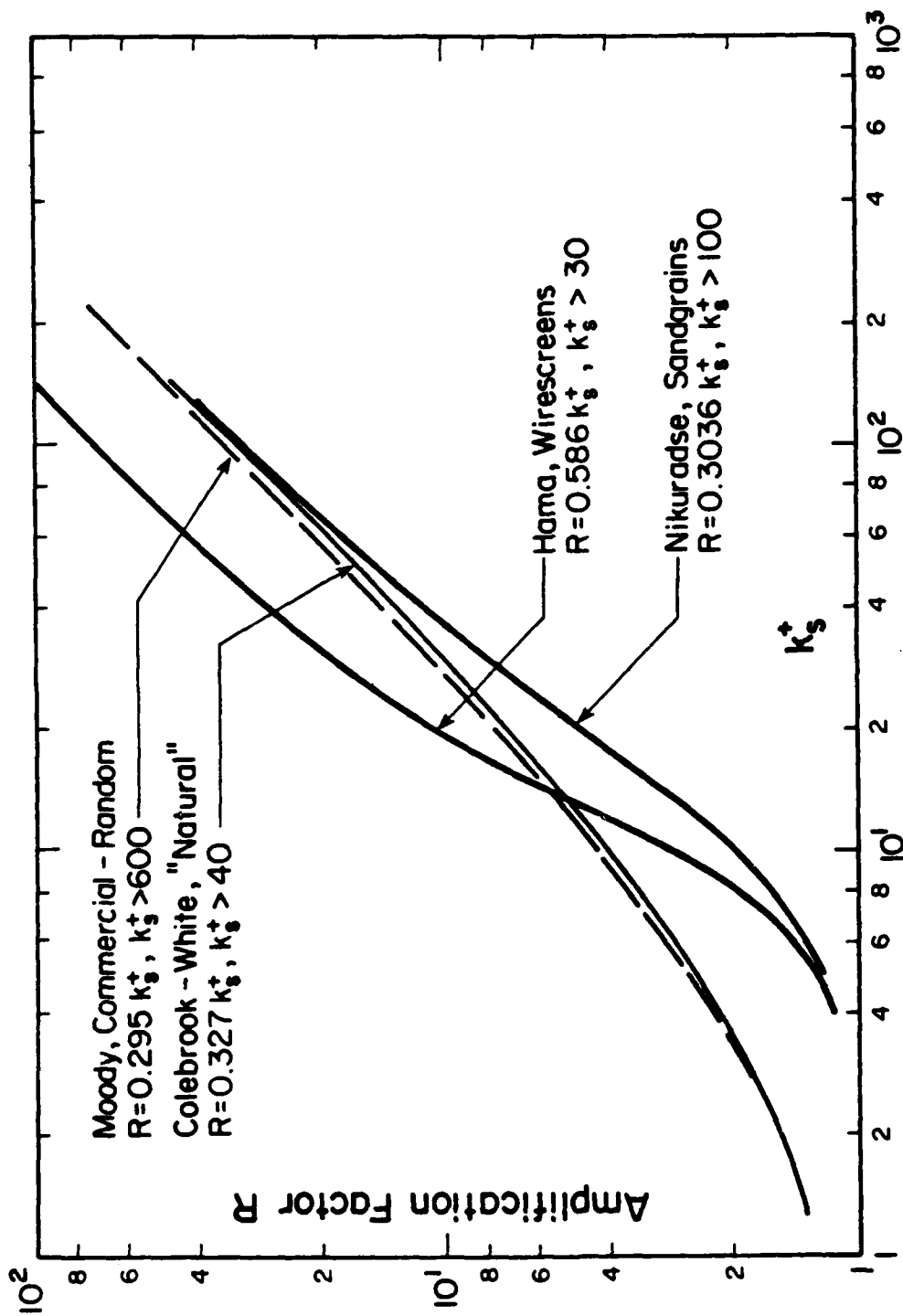


Figure 8b Mixing Length Amplification vs. Surface Roughness



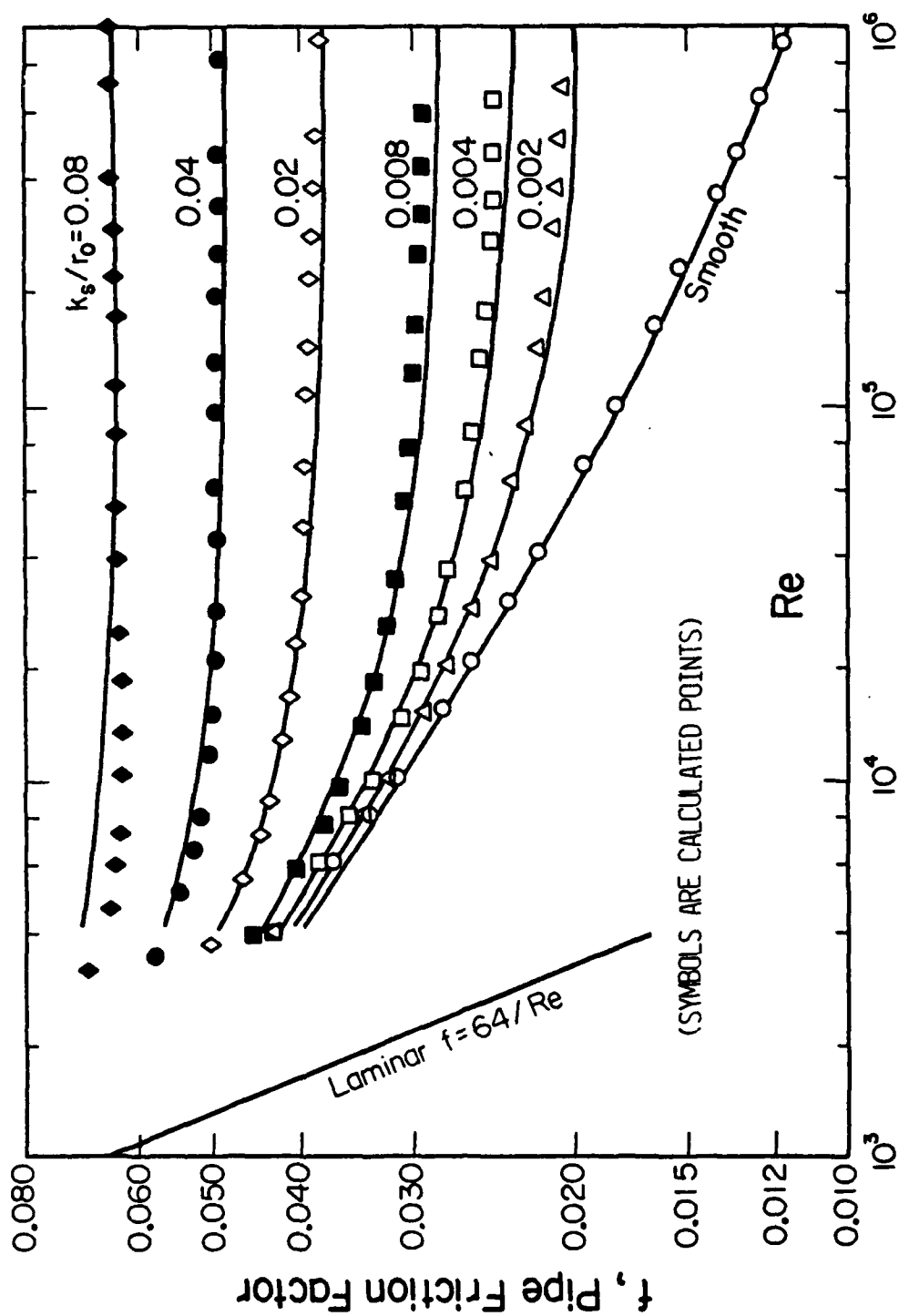


Figure 9 Calculated Pipe Friction Factors for Commercial-Random Roughnesses, Moody

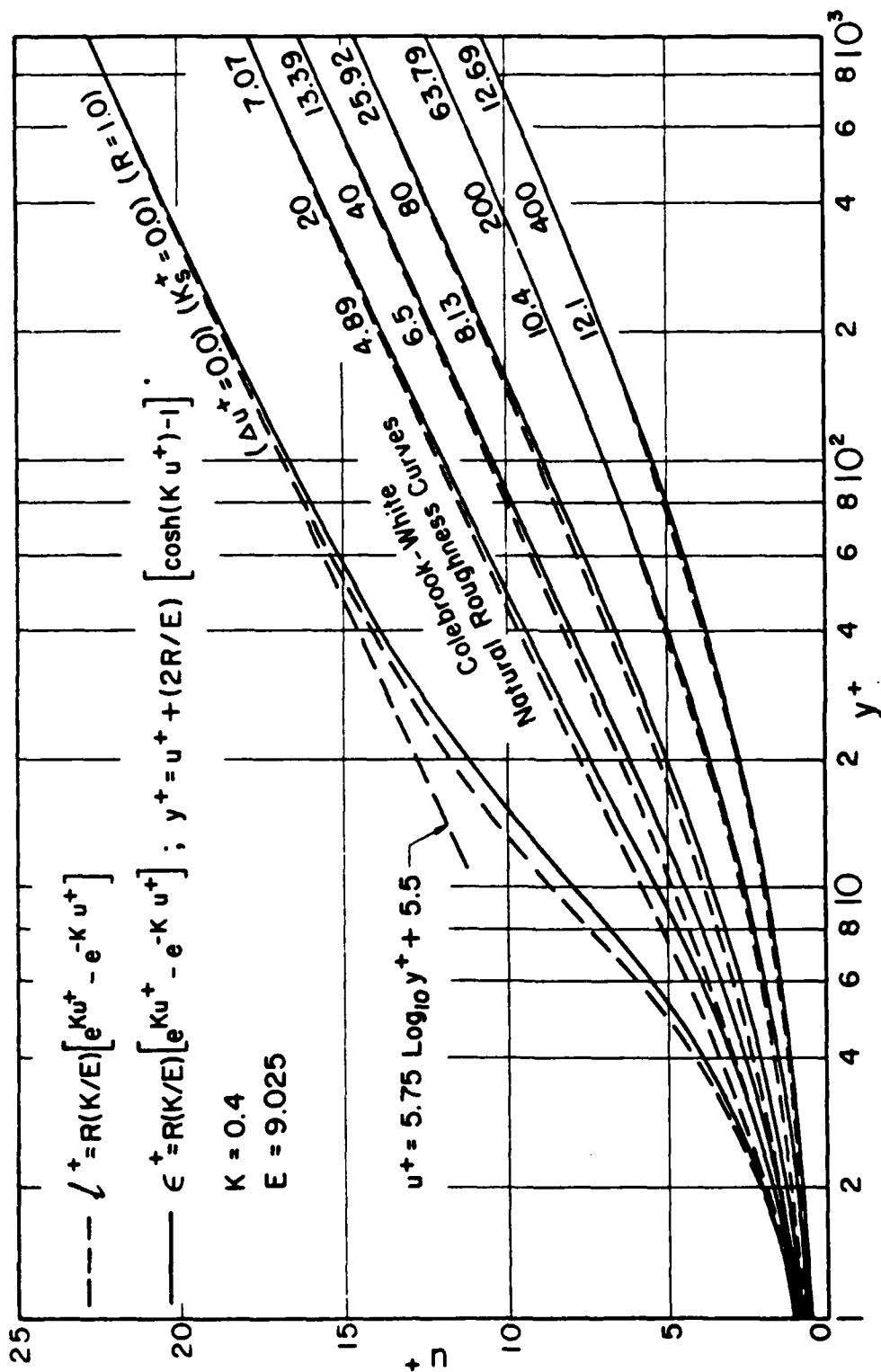


Figure 10 Wall-Region Velocities for Rough Surfaces (Colebrook-White)

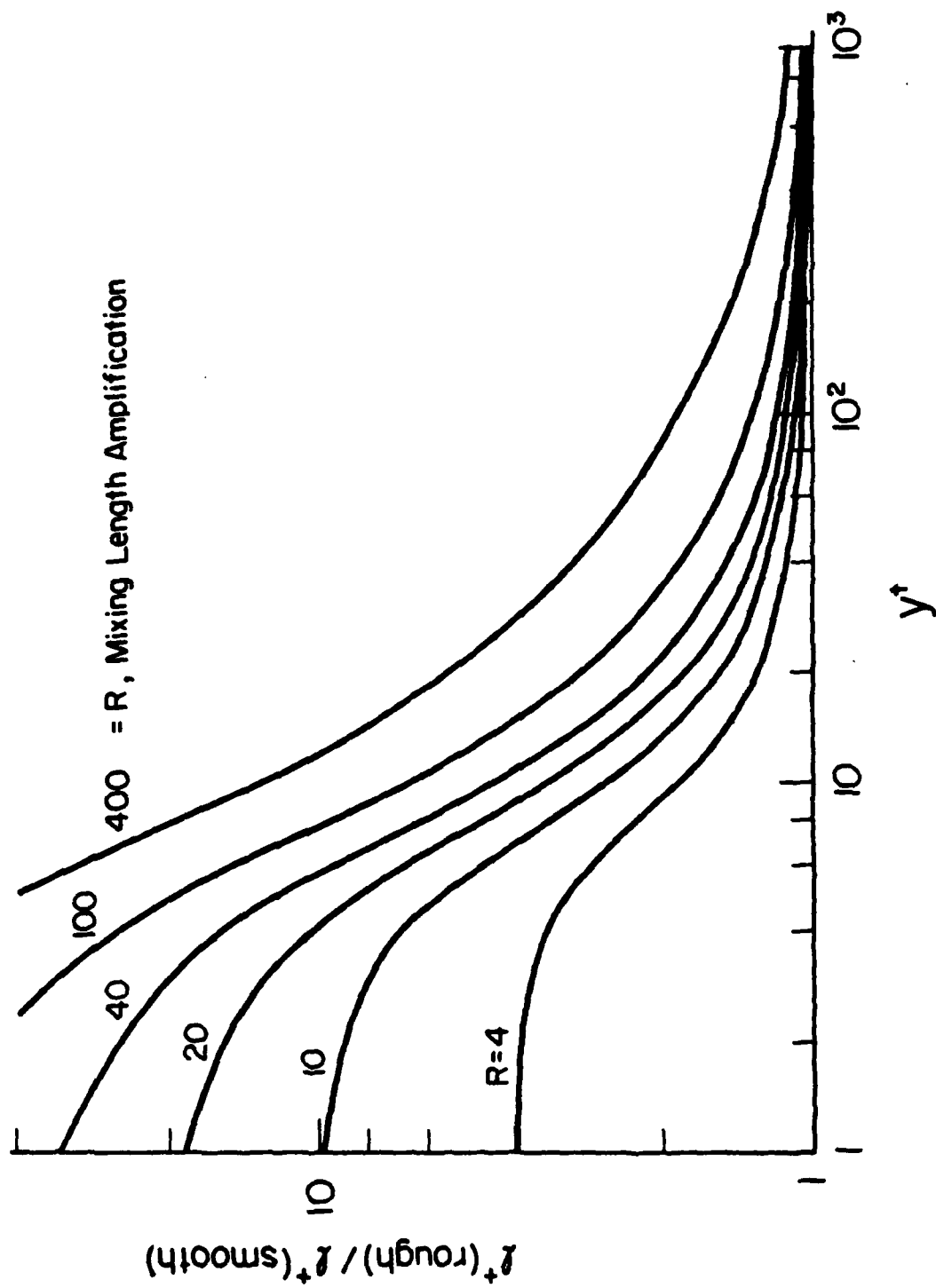


Figure 11 Spatial Distribution of Rough-to-Smooth Mixing Length Ratio

Table 1. Mixing Length Amplification for Sandgrain (Nikuradse)  
and Commercial Random (Moody) Roughnesses.

$k_s^+$	Nikuradse' Sandgrains	Moody's Commercial Random
0.0	1.	1.
1.0	1.0072	1.1823
2.0	1.0288	1.5173
3.0	1.0663	1.8751
4.0	1.1278	2.2534
6.0	1.3182	2.9576
8.0	1.6059	3.6637
10.0	2.0003	4.3767
12.0	2.4778	5.0748
14.0	2.9973	5.7565
16.0	3.5597	6.4233
18.0	4.1554	7.0854
20.0	4.7771	7.7445
25.0	6.4263	9.3921
30.0	8.1745	11.0470
35.0	9.9698	12.7034
40.0	11.7392	14.3558
45.0	13.4528	15.9967
50.0	15.0897	17.6186
60.0	18.2128	20.8224
70.0	21.2345	23.9910
80.0	24.2704	27.1310
90.0	27.3172	30.2425
100.0	30.3600*	33.3253
120.0		39.4392
140.0		45.5067
160.0		51.5278
180.0		57.5026
200.0		63.4309
300.0		92.7567
400.0		121.4452
500.0		149.4452
600.0		177.0*

\* R becomes linear afterwards:  $R = 0.3036 k_s^+$  (Nikuradse)  
 $R = 0.295 k_s^+$  (Moody)

#### IV. FLOW OVER A ROUGH FLAT PLATE

An underlying reason for developing a rough-surface analytical methodology is its applications to engineering problems. Among these, boundary layer flows are of prime interest. In fact it was to fill this need that led Schlichting [3] to undertake the task of transposing Nikuradse' data on sandgrain roughnesses in pipes to external boundary layer flows. Although such a process of direct transposition needs confirmation or refinement, as observed previously in this work, a graph estimating rough-surface turbulent friction serves well the purpose of, say, marine engineers whose task it is to calculate a ship hull's resistance, or turbine-blade analysts who are to account for the increased frictional losses on eroded blade surfaces.

In its conceptual outline the methodology is complete. Its implementation to surfaces with all types of roughnesses and various flow geometries awaits more extensive efforts which include a more comprehensive compilation of the amplification data, either from currently available information or by further experimentation. In addition, the new model formulation is to be tested and improved upon for flows with such influential parameters as the pressure gradient, blunt nose-region, etc. Only then can a reliable analysis be made with confidence with regard to the rough-surface features over a turbine blade contour. It is to be noted that for smooth surfaces, the relevant flow parameters, such as the pressure gradient, have had a long period of research by way of experimentation and modeling ever since the early evolvement of the Prandtl-van-Driest combination in the fifties. And for rough surfaces, what fraction of the available experience and knowledge obtained on smooth

surfaces can be directly transposed to rough-wall flow problems is not clear without additional efforts.

What is clear, however, is that for the first time, rough-surface boundary layer flows without pressure gradients can be analyzed by a finite-difference scheme - using the modal methodology developed. The choice of a flat-plate configuration without pressure gradient is made on the basis that other flow parameters may become distractive and cloud the focus of a capability demonstration. Furthermore in order to explore the operational features of the model, a simple finite-difference algorithm is preferred and is therefore constructed, instead of using a ready-made, proven program, such as STAN-5 or Cebeci-Smith.

The program utilizes a grid network of two streamwise stations, each containing three transverse grid points. A marching step proceeds from one streamwise station where all the velocities are known to the next station in which the velocities parallel to the surface are the unknown values to be found. Turbulence quantities at the new station take on the values computed for the prior station. In this way, the computational algorithm is a one-step marching implicit method. Other mathematical details are discussed in Appendix A.

Two validation runs are conducted for the computer program: one to verify that Blasius' results for a laminar flat plate flow are reproduced numerically. The second validation run consists of computing the turbulent boundary layer friction based on Prandtl-van-Driest formulation, i.e. Equation (6d) and alternatively based on formulation (iii) of Equation (14), and then comparing the results from the two parallel computations with each other and with the accepted semi-empirical correlation equations. The first test shows some difference between the results: the discrepancy

is limited to a starting region of  $Re_x = 10^4$  and less, and is principally caused by the initiating velocity profile at the leading edge which is uniform but contains no transverse velocities. In the second test run, computations were conducted without the use of a "wall-function" and shear stresses on the plate surface were directly obtained by calculating the velocity gradient on the surface. The calculated values of friction based on the currently used zero-equation model, i.e. Prandtl-van-Driest, and based on the new model of this work are very compatible with each other. Differences are there but only in the range of 1 percent or less with each other. The calculated results from either basis are in excellent accord with the accepted correlation equations for smooth surfaces shown below:

$$Re_x C_f = 0.324[1 - 8.125 \sqrt{C_f} + 22.08 C_f] \exp(.58/\sqrt{C_f}) \quad (41)$$

and

$$C_f = 0.0592/Re_x^{0.2} \quad (42)$$

These two equations are given in Cebeci-Smith [11] and in Schlichting [3]. The simpler Equation (42) has a range of validity limited to  $Re_x = 10^7$  whereas the former equation has a greater range.

Roughness Effect on Friction Coefficient. Results obtained for a smooth-surface flat plate using mixing length formulation (iv) of Equation (14) are shown as circle-symbols in Figure 12, in which correlation of the computed results with Equations (41) and (42) is self-evident.

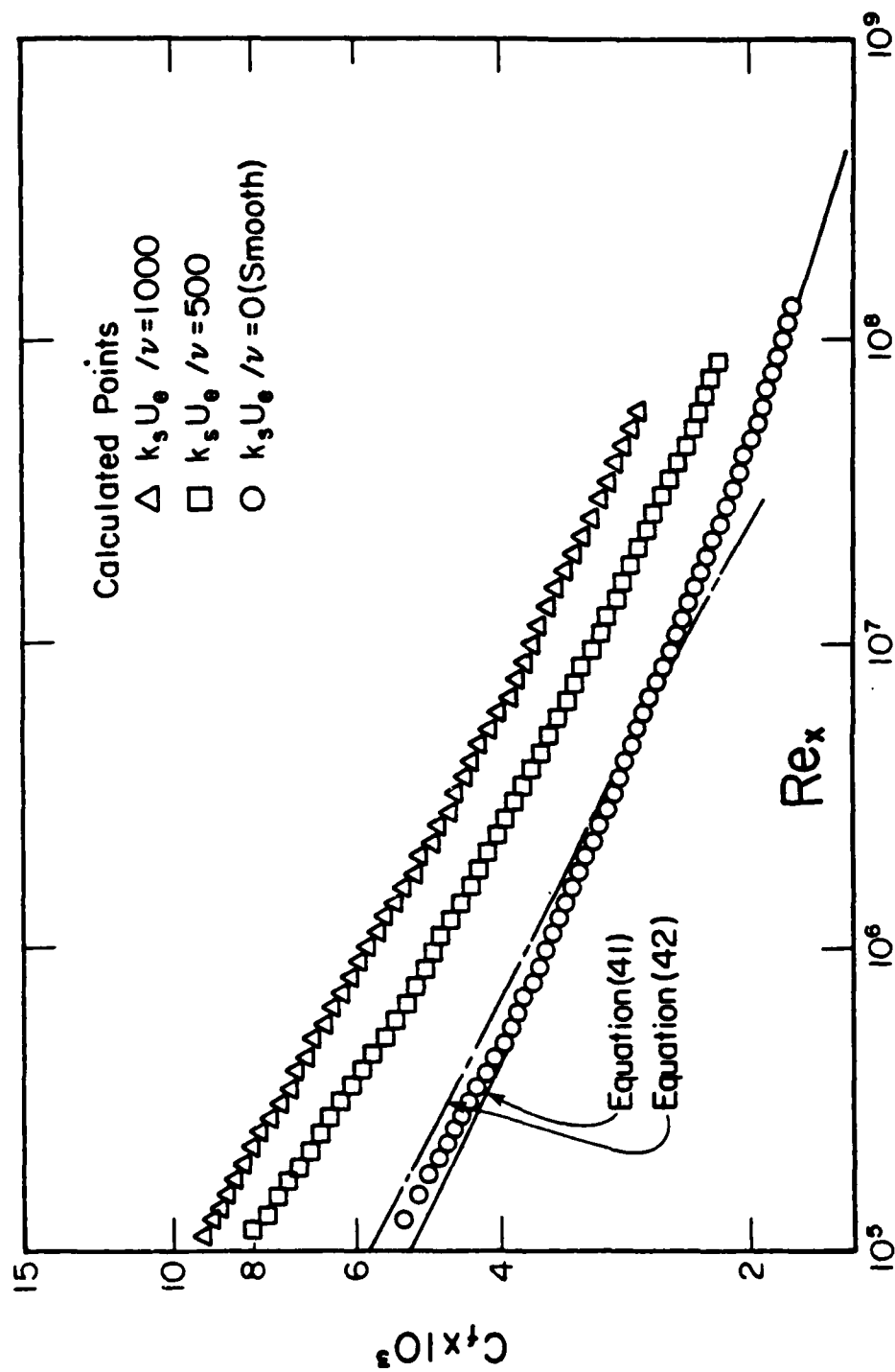


Figure 12 Calculated Local Friction Coefficients on Flat Plates with Nikuradse' Sandgrain Roughnesses ( $K = 0.41$ ,  $E = 7.768$ )



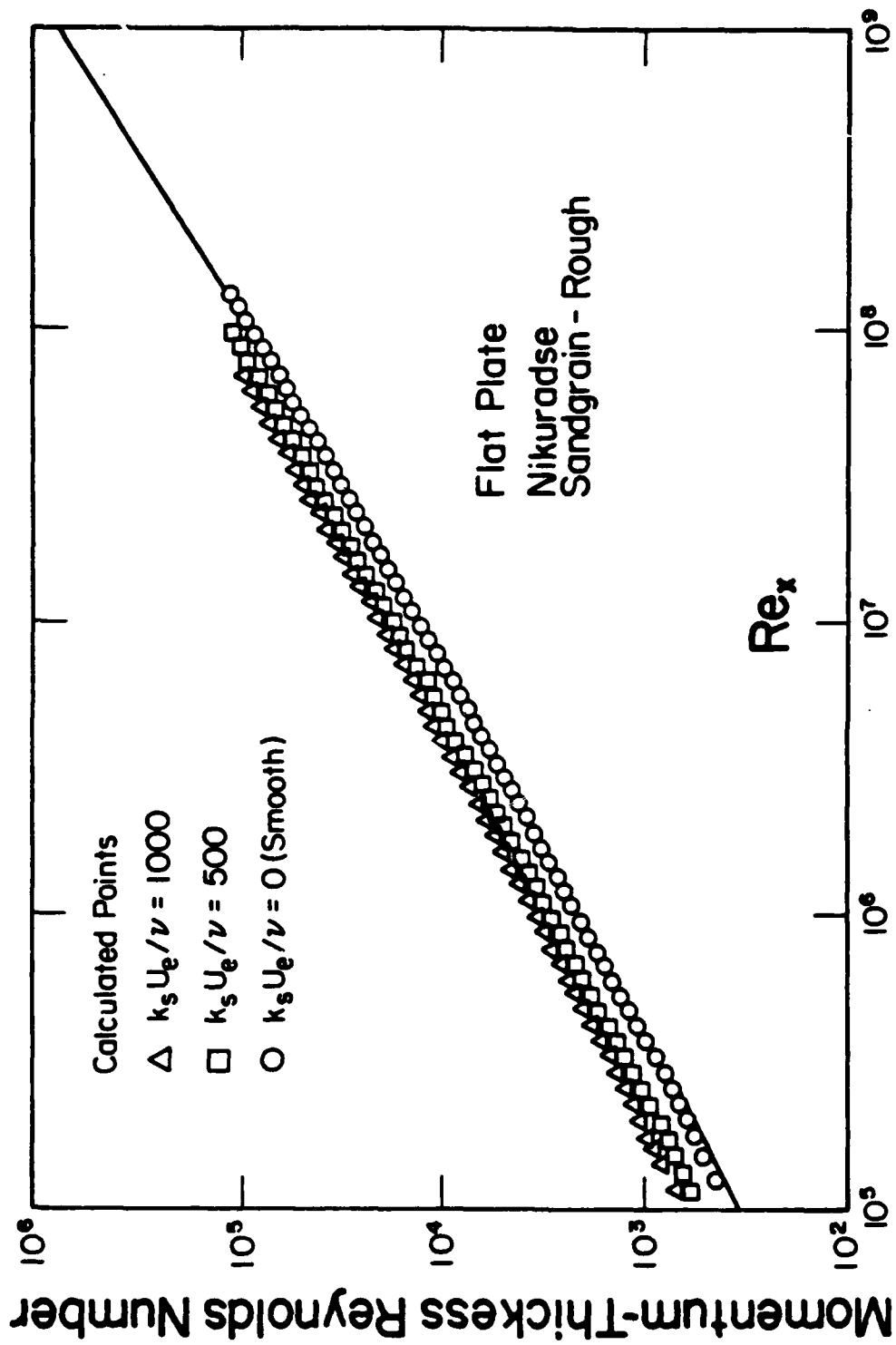


Figure 13 Calculated Momentum Thicknesses vs. Reynolds Numbers with

Nikuradse' Sandgrain Roughnesses ( $K=0.41$ ,  $E=7.768$ )

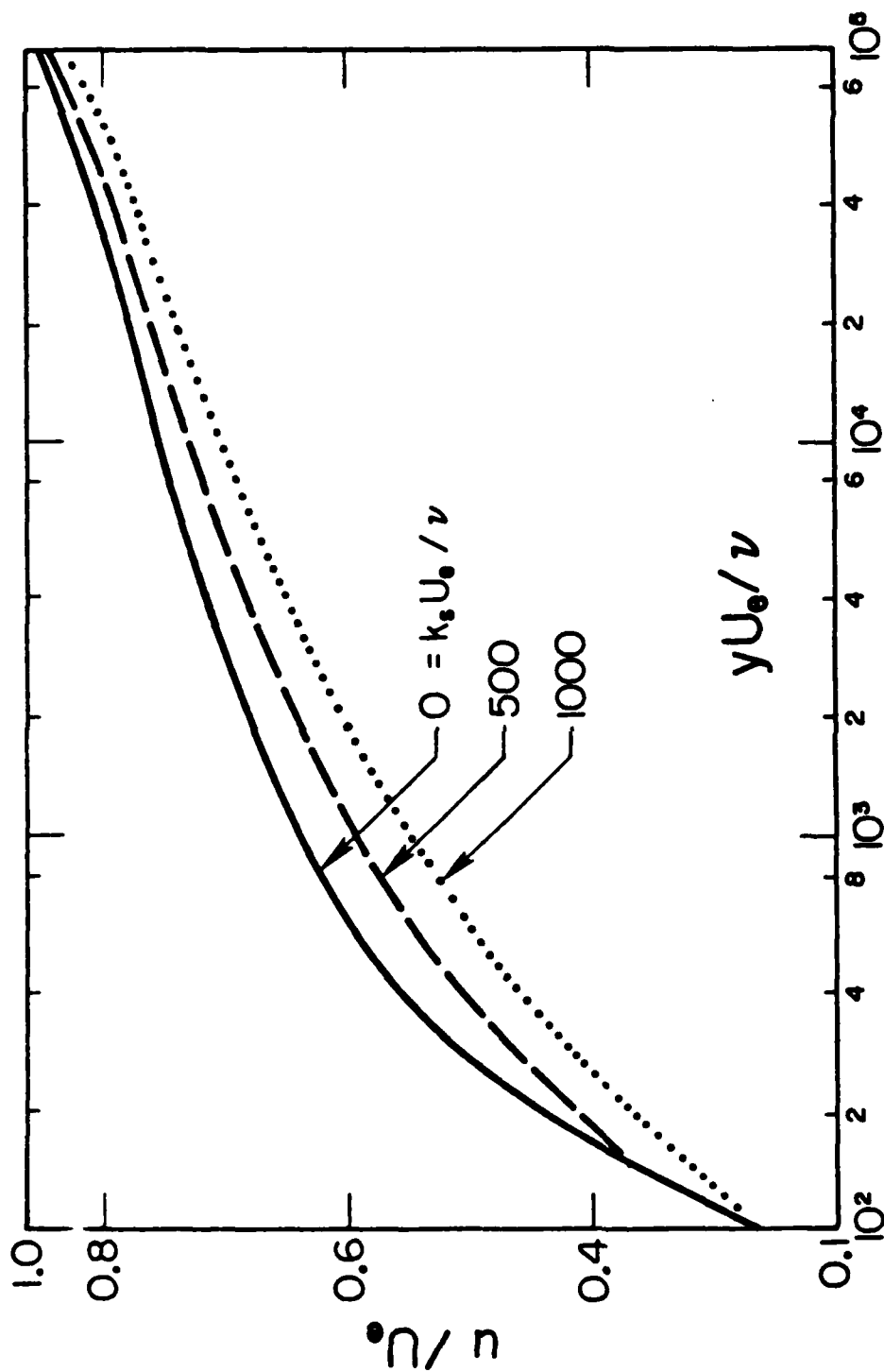


Figure 14 Calculated Rough-Surface Boundary Layer Velocity Profiles at

$Re_x = 10^7$ , Boundary-Layer Coordinates ( $K=0.41$ ,  $E=7.768$ )

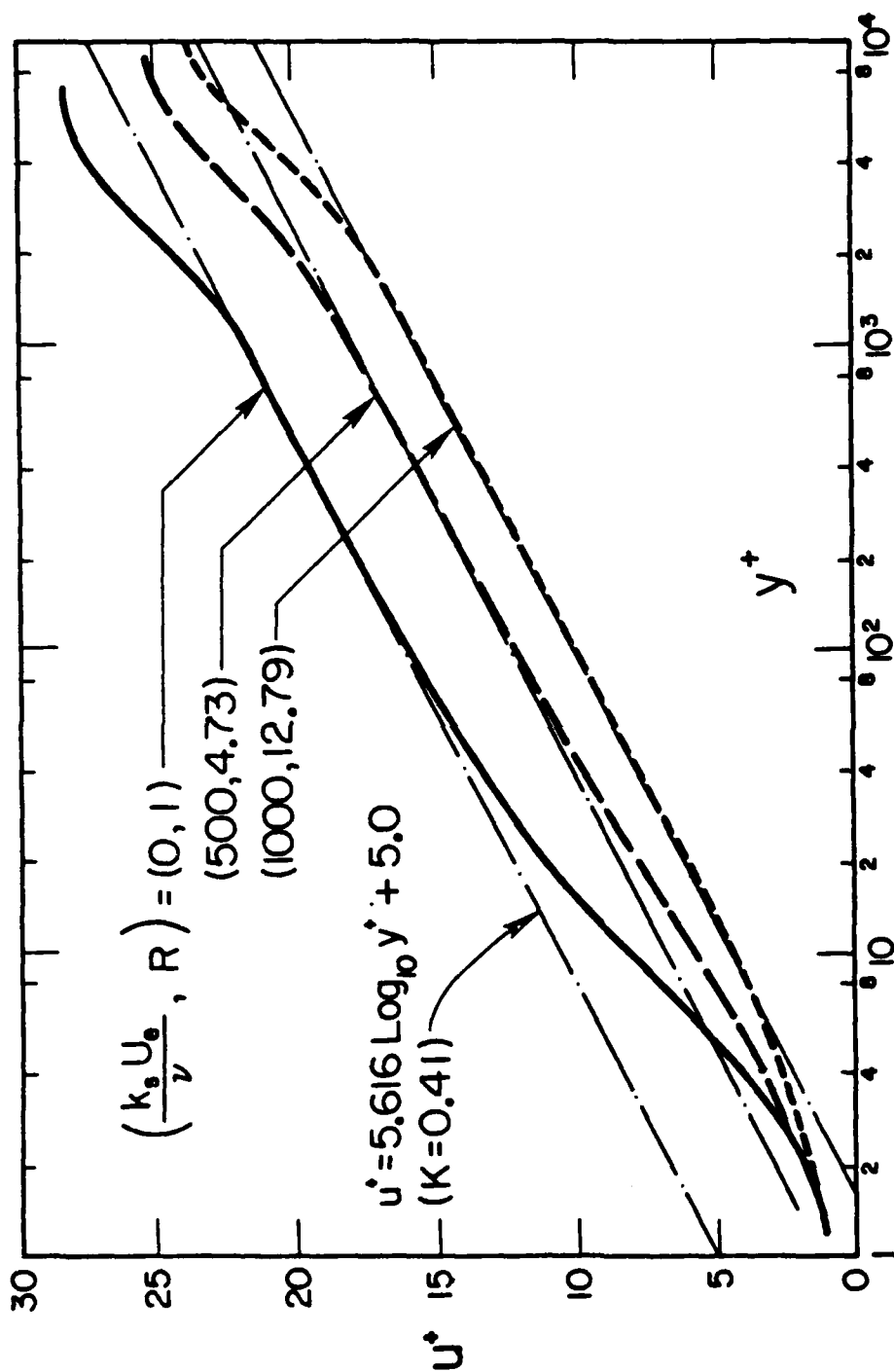


Figure 15 Calculated Rough-Surface Boundary Layer Velocity Profiles at

$Re_x = 10^7$ , Plus-Coordinate ( $K=0.41$ ,  $E=7.768$ )

In commencing the analysis, the roughness Reynolds number cannot be specified in advance, for it contains a friction velocity which is not known a priori. In fact it varies along the flat surface as the turbulent boundary layer grows, and becomes progressively smaller thus mitigating the effect of the surface protrusions at large distances from the leading edge.

Instead, a roughness-freestream Reynolds number ( $k_s U_e / \nu$ ) can be specified and used as a calculation parameter. Two values are assigned in this set of calculations: 500 and 1000. (For a smooth surface, it corresponds to a zero-value.) Even for a higher value of 1000, it represents a conservative estimate of the roughness height. Consider a turbine blade with a chord length of 5 inches and a chord Reynolds number of  $10^7$ ; a roughness-freestream Reynolds number of 1000 is translated into a ratio of roughness height to chord length of  $10^{-4}$ . Physically, this ratio is equivalent to an average surface irregularity of 0.0005 inches, a reasonable dimension for an eroded surface indeed.

Finite-difference calculations in the demonstrative runs proceed from the leading edge of the flat, starting with a uniform velocity profile but with no transverse velocity component; computations are terminated at a length Reynolds number approximately  $10^8$ . During the marching process, friction is calculated by the velocity derivative on the surface through a three-point formula rather than a "wall-function" technique; the latter technique is often used to economize computation time and is only valid if the sublayer variation in the boundary layer is an established phenomenon, as is the case for smooth surfaces. Computed surface shear is transformed into a friction velocity which, when combined with the roughness-freestream Reynolds number, gives the roughness Reynolds number  $k_s^+$  and thence the

amplification factor  $R$ . Data of  $R$  vs  $k_s^+$  for Nikuradse' sandgrain roughnesses are used in the illustrative calculations.

Boundary layer characteristics for the three roughnesses specified by  $(k_s U_e / \nu) = 0, 500$  and  $1000$  are shown in Figure 12 for the friction coefficient distributions and in Figure 13 for the momentum-thickness Reynolds numbers along the plate positions  $Re_x$ . Results shown in Figure 12, where the calculated variations are indicated by the symbols, warrant the following observations:

- (i) The increase of surface friction is very significant. At  $Re_x = 10^7$  and  $(k_s / x) = 10^{-4}$  corresponding to  $(k_s U_e / \nu) = 1000$ , the local friction value is 60 percent more than a smooth plate value, a change too appreciable to ignore.
- (ii) The computed results, although compatible qualitatively with the transposed graph of Prandtl-Schlichting [3], indicate substantial, quantitative deviations from these approximate, transposed data. A re-working of such a skin-friction graph, possibly incorporating the compressibility or Mach number effect, is now possible and constitutes a more rational base.

Finite-difference calculations also yield the momentum and displacement thickness variations along the flat plate surface. For the displacement thickness, the increase from a smooth-surface to a rough-surface value, caused mainly by the velocity retardation in the main body of the boundary layer over a rough surface, is much more pronounced than for the momentum thickness change. Thus for rough-wall boundary

layers, the shape factors are quite different from those for smooth surfaces. Figure 13 shows the variations of momentum thicknesses for the three roughnesses investigated. The variation for smooth surfaces matches with the established correlation well - indicated by the line in the figure.

Velocity Distribution Across Rough-Surface Boundary Layers. In order to bring out as much as possible the operational features of the method, the velocity distributions for the three roughness-freestream Reynolds number  $(k_s U_e / \nu) = 0, 500$  and  $1000$  at a local Reynolds number  $Re_x = 10^7$  are displayed. These velocities are those that occur at a single plate location, but because of different surface conditions, exhibit different distributions. Shown in Figure 14 are the distribution curves expressed in the boundary layer coordinates, which are common to all three calculations, and therefore the curves show their relative magnitudes. Apparent from inspecting Figure 14 is the fact that over almost the entire boundary layer thickness, the rough-surface velocity distribution becomes progressively lower as the surface becomes rougher. Only in a very narrow band,  $(y U_e / \nu) < 100$ , is this relative velocity difference reversed, i.e. the smoother is the surface the lower is the velocity - just the opposite in the overwhelming portion of the boundary layer. The reversal in their relative values, which occurs mainly in the sublayer region, is prominent enough in the graph to discern, even though the near-wall portions of the curves are not shown for compactness.

Re-presenting the same velocity distributions using the plus-coordinates gives the curves shown in Figure 15. It must be noted that in non-dimensionalizing the results, the surface shear actually

calculated is used to compute  $u_\tau$ , the friction velocity which is a part of the plus-coordinate structure. The display in Figure 15 shows excellent matching with the wall-law slope for the three distributions, and they all converge to a single curve of slope of unity for  $y^+ < 2$ , a condition that cannot be satisfied by prior modeling efforts. The relative levels of the wall-law region curves are reflected through the different values for the amplification factor  $R$  noted in Figure 15.

## V. CONCLUSIONS

Completed in this investigation is a methodology which allows the analysis and calculation of the turbulent boundary layer development over a rough surface. It is a zero-equation model and consists of two fundamental building blocks: the first one is the well-established Prandtl's mixing length hypothesis but expressed in the methodology by a function of the velocity-space variable  $u^+$  instead of the physical-space variable  $y^+$ .

The mixing length expressed in  $u^+$  is, in the context of the methodology, multiplied by a constant factor - the amplification factor for surface roughness - while the experimental manifestations of rough-wall boundary layer flows are all satisfied. The use and extraction of the amplification factor values at different and various kinds of surface roughnesses constitute the second building block of the methodology.

To provide an empirical link between  $R$  and  $k_s^+$ , four kinds of surface roughnesses are analyzed in this work. Based on the available experimental data, the amplification factor for each is presented as a function of the roughness Reynolds number. These four kinds are Nikuradse's sandgrains, Hama's wirecreens, Colebrook-White's mixed sands and Moody's commercial random. And they can be grouped into two categories - one with a uniform texture and the other with a randomly distributed roughness of various sizes. To the first category belong the experimental data of Nikuradse and of Hama's wirescreen tests. Moody's compilation of friction data in commercial pipes and Colebrook-White's collection for surfaces coated with sand mixtures constitute the second group.

The variations of the amplification factor with the surface roughness size characterize the contrasting manifestations of those two groups as is



evidenced in Figures (8a) and (8b). For the group with uniform textures, the amplification factor rises but slowly at low values of the surface roughness factor, thus constituting a dormant regime which is referred to in the literature as "hydraulically smooth". As the surface roughness increases beyond a somewhat murky threshold value, the amplification factor becomes a linear function of the surface roughness. Phenomenologically, this may be interpreted as the vortex region, as the flow near the surface asperities is comprised of continual shedding of separation vortices. In the literature, this regime is termed fully rough regime. The intermediate zone between these two is a transitional regime in which vortices are beginning to shed in an onset manner - the burst region.

For roughnesses of the second category, i.e. those with random mixtures of various sizes, the amplification factor rises almost linearly without passing through the first two regimes.

These fundamental observations underscore the need to investigate other parametric factors. For a more comprehensive treatment of the new methodology, extensions to flows with pressure gradients, etc. are required. This is reflected in its analytical counterpart for smooth surfaces. Extensive refinements have been carried out in modifying van Driest's damping constant to include effects such as surface blowing and pressure gradients. Similar efforts are recommended for the new model formulation applicable to rough surfaces.

Pertaining to the second building block, the amplification versus roughness relation, survey of available data on surface roughnesses of the types other than the ones treated is warranted. Alternatively, direct experimentation should be conducted with a view to obtain the amplification factors. Then, there are other geometrical factors with regard to the type

of roughness; these are the spatial dispersal, two- or three-dimensional distribution patterns and others.

## REFERENCES

1. Bakhmeteff, B.A., The Mechanics of Turbulent Flow, Princeton University Press, 1941.
2. Moody, L.F., "Friction Factors for Pipe Flow," Trans. ASME, Vol. 66, p. 671, 1944.
3. Schlichting, H., Boundary Layer Theory, McGraw-Hill Book Co., 6th Edition, 1968, p. 583.
4. Bammert, K., and Sandstede, H., "Measurements Concerning the Influence of Surface Roughness and Profile Changes on the Performance of Gas Turbines," J. of Eng. for Power, July 1972, p. 207-213.
5. Coles, D., "A Survey of Data for Turbulent Boundary Layers with Mass Transfer," AGARD Conference Proceedings 93, London, 1971.
6. van Driest, E., "On Turbulent Flow Near a Wall," J. Aero. Sci., Vol. 23, p. 1007, 1956.
7. Coles, D., "The Law of the Wake in the Turbulent Boundary Layer," J. Fluid Mech., Vol. 1, p. 191, 1956.
8. McDonald, H., and Fish, R.W., "Practical Calculations of Transitional Boundary Layers," Int. J. Heat Mass Transfer, Vol. 16, p. 1729-1744, 1973.

9. Healzer, J.M., Moffat, R.J., and Keys, W.M., "The Turbulent Boundary Layer on a Porous, Rough Plate: Experimental Heat Transfer with Uniform Blowing," AIAA Paper No. 74-680, Thermophysics and Heat Transfer Conference, Boston 1974.
10. Rotta, J., "Turbulent Boundary Layers in Incompressible Flows," Progress in Aero. Sci., Vol. 2, p. 1, 1962.
11. Cebeci, T., and Smith, A.M.O., Analysis of Turbulent Boundary Layers, Academic Press, 1974.
12. Momoh, S.K., "An Eddy-Viscosity Approach to the Calculation of Velocity and Heat-Transfer Properties of Flow in Rough Pipes," Letters in Heat and Mass Transfer, Vol. 6, p. 125-130, 1979.
13. Spalding, D.B., "A Single Formula for the Law of the Wall," J. of Appl. Mech., p. 455, September 1961.
14. Kleinstein, G., "Generalized Law of the Wall and Eddy-Viscosity Model for Wall Boundary Layers," AIAA, Vol. 5, p. 1402, 1967.
15. Eckert and Drake, Heat and Mass Transfer, McGraw-Hill Book Company, 1972.
16. Robertson, J.M., et. al., "Turbulent Flow in Rough Pipes," Ind. & Engr. Chem. Fundamentals, Vol. 7, p. 253, 1968.

17. Ross, Donald, "A New Analysis of Nikuradse's Experiments on Turbulent Flow in Smooth Pipes," Proceedings of 3rd Midwestern Fluid Mechanics Conf., 1952, Columbus, Ohio.
18. Lakshman, C. and Jayatilke, V., "The Influence of Prandtl Number and Surface Roughness on the Resistance of the Laminar Sublayer to Momentum and Heat Transfer," Prog. Heat Mass Transfer, Vol. 1, p. 193, 1969.
19. Colebrook, C.F., and White, C.M., "Experiments with Fluid Friction in Roughened Pipes," Proc. Roy. Soc. of London, A161, p. 367, (1937).
20. Hama, F.R., "Boundary Layer Characteristics for Smooth and Rough Surfaces," Trans. Soc. Naval Arch. & Marine Engrs., Vol. 62, p. 333, 1954.

## APPENDIX

### COMPUTER PROGRAM FOR TURBULENT BOUNDARY LAYER ANALYSIS

The computer program used in this investigation has a specific purpose of calculating the turbulent boundary layer characteristics for flow over rough surfaces. Speed and time-economy are not the principal attributes required of the algorithm, nor is its comprehensiveness in admitting other flow conditions or specifications, for it is essentially a validation device to explore the performance of the new formulation of mixing length which can incorporate surface roughness in the model. In keeping with this objective, a flat plate configuration without pressure gradients and for an incompressible fluid of constant physical properties is therefore adopted. Further, in order to avoid the question of laminar-to-turbulent transition - which is a separate issue - the flow is assumed to be turbulent right at the leading edge station.

In this simplified context, the velocity components  $u$  and  $v$  along the plate-surface ( $x$ ) and transverse ( $y$ ) directions are first transformed into dimensionless forms by:

$$\begin{aligned}\bar{x} &= xU_e/\nu \\ \bar{y} &= yU_e/\nu \\ \bar{u} &= u/U_e \\ \bar{v} &= v/U_e \\ \bar{\delta}_1 &= \delta_1 U_e/\nu.\end{aligned}\tag{A-1}$$

All symbols are defined in the Nomenclature section except  $\delta_1$  which is the displacement thickness of the boundary layer. The boundary layer equation and the conservation equation in terms of the bar-coordinates, i.e. the boundary layer coordinates, are expressed by:

$$u \frac{\partial \bar{u}}{\partial \bar{x}} + \bar{v} \frac{\partial \bar{u}}{\partial \bar{y}} = \frac{\partial}{\partial \bar{y}} \left[ (1 + \epsilon^+) \frac{\partial \bar{u}}{\partial \bar{y}} \right] \quad (\text{A-2})$$

$$\frac{\partial \bar{u}}{\partial \bar{x}} + \frac{\partial \bar{v}}{\partial \bar{y}} = 0. \quad (\text{A-3})$$

The boundary conditions associated with these equations are

- (a)  $\bar{u} = 1$  at  $\bar{x} = 0$  and at  $\bar{y} = \infty$
- (b)  $\bar{u} = 0$  at  $\bar{y} = 0$
- (c)  $\bar{v} = 0$  at  $\bar{y} = 0$ .

The boundary layer turbulence is embedded in  $\epsilon^+$  of Equation (A-2) which denotes the ratio of a turbulent viscosity to the molecular viscosity, i.e.

$$\epsilon^+ = \mu_t / \mu. \quad (\text{A-4})$$

Two turbulence models are used in calculating  $\epsilon^+$ : one is the widely accepted Prandtl-van-Driest prescription for smooth surfaces and is defined by Equation (6d) for mixing length; the other model uses an exponential expression in  $u^+$  for mixing length and is given by formulation (iv) of Equation (14), or Equation (40), which contains an amplification factor  $R$  depending on the surface roughness size. For empirical constants  $K$  and  $E$

in these model equations, 0.41 and 7.768 are used; the latter value corresponds to  $C = 5$  in Equation (1).

Turbulence quantities which confine their activities in the near-wall region of the boundary layer are characterized by the friction velocity  $u_t$  defined by

$$u_t = \sqrt{\tau/\rho}, \quad (A-5)$$

where  $\tau$  is the surface shear stress. The surface shear is calculated by the velocity gradient on the surface multiplied by the molecular viscosity since the turbulent viscosity is zero on the surface. The friction velocity  $u_t$  in Equation (A-5) is made dimensionless by the external freestream velocity  $U_e$ ,

$$\bar{u}_t = u_t/U_e. \quad (A-6)$$

Equations (A-1) and (A-6) contain all the dimensionless variables in the boundary-layer coordinates needed in this work. In the calculation of the turbulence quantities, a new coordinate system - the plus coordinates - is required in the scaling process. The relevant plus-coordinate variables are:

$$\begin{aligned} u^+ &= u/u_t \\ y^+ &= yu_t/\nu \\ l^+ &= lu_t/\nu. \end{aligned} \quad (A-7)$$



Through these variables and for each turbulence model, the turbulent viscosity  $\epsilon^+$  calculated by the equation for each increases as the distance from the wall increases. In the outer region where the scaling variable for velocity becomes the freestream velocity  $U_e$ , the turbulent viscosity  $\epsilon^+$  is not to exceed the limit set by

$$\epsilon^+ = 0.0168 \bar{\delta}_1 \quad (A-8)$$

which is widely accepted in the zero-equation model for turbulent flow calculations. The two dimensionless coordinate systems are connected by the following,

$$\begin{aligned} u^+ &= \bar{u} / \bar{u}_t \\ y^+ &= \bar{y} \bar{u}_t \end{aligned} \quad (A-9)$$

The Finite-Difference Algorithm. A unit grid network consisting of three transverse nodes in each of the two streamwise stations is shown in Figure A-1. Transverse to the surface, the nodes are spaced apart in a geometrical progression for the successive spacings between neighboring nodes. Between the wall-node and the adjacent node, the distance expressed in the boundary layer coordinate  $\Delta \bar{y}$  is usually set between 10 and 20. Expressed in the plus-coordinates, this initial spacing is equivalent to  $\Delta y^+ = 0.5$  to 1, a reasonably small step in the integration process.

In the transverse direction the successive spacings grow in a geometrical ratio of 1.07, an optimum value for speed and storage economy. All together 600 transverse nodes are allowed and only two hundred are ever needed. The boundary layer calculation starts at the leading edge position

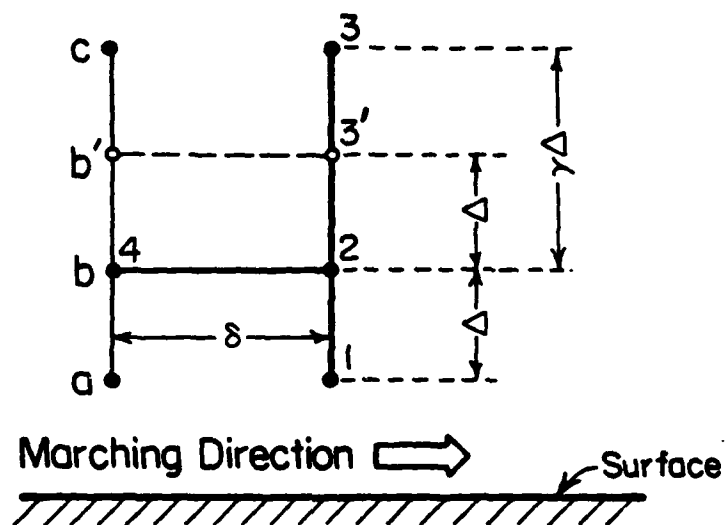


Figure A-1 Grid Network for 3-Point 2-Station Marching

with a uniform velocity with only 100 nodal positions; more nodal points are added one at a time when the outer-most node has a velocity equal to or less than 0.999.

The left-hand side of boundary layer Equation (A-2) is replaced by the following term-by-term approximations involving the values at the nodal points of Figure A-1:

$$\bar{u} \frac{\partial \bar{u}}{\partial x} = \bar{u}_b (\bar{u}_2 - \bar{u}_b) / \delta \quad (A-10)$$

$$\bar{v} \frac{\partial \bar{u}}{\partial y} = \bar{v}_b (\bar{u}_3 - \bar{u}_1) / (2\Delta), \quad (A-11)$$

where all subscripts refer to the nodal positions indicated in Figure A-1. The transverse spacing  $\Delta \bar{y}$  is denoted by  $\Delta$  and the streamwise spacing  $\Delta \bar{x}$  by  $\delta$ . For the right-hand side of Equation (A-2), it is first decomposed into two parts:

$$(1 + \epsilon^+) \frac{\partial^2 \bar{u}}{\partial \bar{y}^2} + \left[ \frac{\partial \epsilon^+}{\partial \bar{y}} \right] \left[ \frac{\partial \bar{u}}{\partial \bar{y}} \right], \quad (A-12)$$

in which the velocity-derivatives are based on the nodal values at points 1,2,3' while the turbulence-viscosity derivatives are based on those at points a,b, and c'. In the computational program, values at the regular nodal points, 1,2,3,a,b, and c are actually used and those at 3' and c' are obtained by a parabolic interpolation scheme. A sample of the interpolation is given by

$$f_{c'} = \frac{2}{\gamma(1+\gamma)} [f_c + (\gamma^2 - 1)f_b - \gamma(\gamma - 1)f_a/2]. \quad (A-13)$$

In other words, having expressed the values at  $c'$  and  $3'$  in terms of values at the regular nodes, the terms of Equation (A-12) can be written as

$$\begin{aligned} & (1 + \epsilon_b^+) (\bar{u}_3 - 2\bar{u}_2 + \bar{u}_1) / \Delta^2 \\ & + (\epsilon_c^+ - \epsilon_a^+) (\bar{u}_3 - \bar{u}_1) / (4\Delta^2). \end{aligned} \quad (A-14)$$

After substituting the finite-difference replacements Equations (A-10), (A-11) and (A-14), a finite-difference equation is obtained which can be written in the index notation in place of the nodal positions of 1, 2, and 3. With the fulcrum point 2 replaced by the index  $i$ , the finite-difference equation with three unknown velocities  $\bar{u}_{i-1}$ ,  $\bar{u}_i$  and  $\bar{u}_{i+1}$  can be written as

$$(\alpha_i) \bar{u}_{i-1} + (\beta_i) \bar{u}_i + (\gamma_i) \bar{u}_{i+1} = \phi_i. \quad (A-15)$$

For each node  $i$ , there is an equation of the form given by Equation (A-15). Since the index starts from 2, (the wall node is designated no. 1), Equation (14) represents a set of linear simultaneous algebraic equations for the index  $i$  varying from 2 to  $(n-1)$ ,  $n$  being the last node count which has a velocity equal to the freestream velocity. Thus, for the index equal to 2, the first equation has only two terms since  $\bar{u}_1 = 0$  at the wall; and similarly for  $i = (n-1)$ , the last equation of the group has but two terms since  $\bar{u}_n$  equals the freestream velocity, a known value, which is lumped to the term

$\phi_{n-1}$  on the right-hand side of the equation. Equations (A-15) therefore form a tri-diagonal matrix equation for which the unknown column matrix  $\bar{u}_2 \dots \bar{u}_{n+1}$  can be found by a simple standard inversion routine.

The Transverse Velocity  $\bar{v}$ . The transverse velocity components at grid points 1, 2, and 3 are found by the following difference-approximations for the derivatives

$$\frac{\partial \bar{u}}{\partial x} = (\bar{u}_2 - \bar{u}_b) / \delta$$

$$\frac{\partial \bar{v}}{\partial y} = (\bar{v}_2 - \bar{v}_1) / \Delta$$

which result in an expression of  $\bar{v}_2$  in terms of  $\bar{v}_1$  and other known quantities,

$$\bar{v}_2 = \bar{v}_1 - (\Delta / \delta) (\bar{u}_2 - \bar{u}_b). \quad (A-16)$$

Since the streamwise velocities  $\bar{u}_i$  have been found, the above equation can be used to compute the transverse velocity  $\bar{v}_2$ , starting with  $\bar{v}_1 = 0$  at the wall, and so on until the entire boundary layer thickness is covered.

Other Facets. Although implicit marching schemes are known to be stable, the marching step used in the program is kept reasonably small - not for time saving but for solution accuracy. The marching step measured in the boundary-layer coordinate  $\bar{x}$  is based on the relation

$$\Delta \bar{x} = 5 (\Delta \bar{y})^2_1, \quad (A-17)$$

where  $(\Delta \bar{y})_1$ , represents the first transverse spacing of the grid, usually set at about 10 to 20. Then,  $\Delta \bar{x} = 800$ , a very small step indeed, if a plate-length Reynolds number of  $10^7$  is to be covered. Equation (A-17) is used over an initial range of  $\bar{x}$  (same as  $Re_x$ ) up to  $\bar{x} = 10^5$  and after that its step size is increased by a factor given by

$$F_x = 5[1 + 5 \tanh^2(\bar{x}/5 \cdot 10^7)]. \quad (A-18)$$

Even with this enlargement factor, a typical number of streamwise steps is in the range 2000 to 5000, thus assuring stability and accuracy.

**END**

**FILMED**

**2-86**

**DTIC**